KfK 3509
Juli 1984

Temperature Escalation in PWR Fuel Rod Simulator Bundles due to the Zircaloy/Steam Reaction: Test ESBU-2A Test Results Report

S. Hagen, H. Kapulla, H. Malauschek
S. O. Peck, K. P. Wallenfels

Hauptabteilung Ingenieurtechnik
Projekt Nukleare Sicherheit

Kernforschungszentrum Karlsruhe

KERNFORSCHUNGSZENTRUM KARLSRUHE
HAUPTABTEILUNG INGENIEURTECHNIK
PROJEKT NUKLEARE SICHERHEIT

KfK 3509

Temperature Escalation in PWR Fuel Rod Simulator Bundles due to the Zircaloy/Steam Reaction: Test ESBU-2A Test Results Report

S. Hagen, H. Kapulla, H. Malauschek, K.P. Wallenfels,
S.O. Peck[+],

[+] USNRC Delegate to Kernforschungszentrum Karlsruhe from EG&G, Idaho Falls, Idaho.

KERNFORSCHUNGSZENTRUM KARLSRUHE GMBH, KARLSRUHE

Kernforschungszentrum Karlsruhe GmbH
ISSN 0303-4003

Summary

This report describes the test conduct and results of the bundle test ESBU-2A, which was run to investigate the temperature escalation of zircaloy clad fuel rods. This investigation of temperature escalation is part of a series of out-of-pile experiments, performed within the framework of the PNS Severe Fuel Damage Program.

The test bundle was of a 3x3 array of fuel rod simulators with a 0.4 m heated length. The fuel rod simulators were electrically heated and consisted of tungsten heaters, UO_2 annular pellets, and zircaloy cladding. A nominal steam flow of 0.7 g/s was inlet to the bundle. The bundle was surrounded by a zircaloy shroud which was insulated with ZrO_2 fiber ceramic wrap.

The initial heatup rate of the bundle was 0.4°C/s. The temperature escalation began at the 255 mm elevation after 1200°C had been reached. At this elevation, the measured peak temperature was limited to 1500°C. It was concluded from different thermocouple results, that induced by this first escalation melt was formed in the lower part of the bundle. Consequently, the escalation in the lower part must be much higher, at least up to the melting temperature of zircaloy. Due to the failure in the steam production system, steam starvation in the upper region may explain the beginning of the escalation at the 255 mm elevation. The maximum temperature reached was 2175°C on the center rod at the end of the test. The unregularities in the steam supply may be the reason for less oxidation than expected.

The posttest appearance of the bundle indicated that molten zircaloy had swept down the cladding oxide layer formed during heatup. The melt dissolved the surface of the UO_2 pellets and refroze as a coherent lump in the lower part of the bundle. The remaining pellets fragmented during cooldown and formed a powdery layer on the refrozen lump.

Temperatureskalation infolge der Zirkaloy/Wasserdampf-Reaktion an Bündeln aus Druckwasserreaktor-Brennstabsimulatoren: Versuchsergebnisse Test ESBU-2A.

Kurzfassung

Dieser KfK-Bericht beschreibt die Versuchsdurchführung und die Ergebnisse des Bündelexperiments ESBU-2A für die Untersuchung der Temperatureskalation von zirkaloyumhüllten Brennelementstäben. Die Untersuchung des Eskalationsverhaltens gehört zum Programm der Out-of-pile Experimente, die im Rahmen der Severe Fuel Damage Untersuchungen des PNS durchgeführt werden.

Das Bündel war in einer 3x3 Anordnung aus unseren üblichen Brennstabsimulatoren aufgebaut. Die Brennstabsimulatoren bestanden aus dem zentralen Heizer, den UO_2-Ringpellets und dem Zirkaloy-Hüllrohr. Das Bündel war von einem Zirkaloy-Vierkantrohr und 6 mm ZrO_2 Faser-Isolation umgeben. Die Länge betrug 40 cm. Der nominelle Dampfstrom durch das Bündel betrug 0.7 g/sec.

Die anfängliche Aufheizrate des Bündels betrug ca. 0.4 °C/sec. Diese Temperatureskalation konnte zuerst in der Meßhöhe 255 mm nach Überschreiten von 1200 °C festgestellt werden. In dieser Höhe erreichte der Eskalationspeak nur 1500 °C. Aus dem Verlauf von Thermoelementmessungen bis ca. 1300 °C konnte geschlossen werden, daß durch den Einfluß der Eskalation im 255 m Bereich sich Schmelze im unteren Bereich gebildet haben muß. Folglich muß sich im unteren Bündelbereich, in dem keine Quotientenpyrometermessungen für die Hochtemperaturbestimmungen durchgeführt wurden, eine deutlich stärkere Temperatureskalation bis mindestens zur Schmelztemperatur des Zirkaloys ausgebildet haben. Die mäßige Eskalation im höheren Bereich des Bündels kann durch Dampfmangel infolge eines Fehlers im Dampfversorgungssystem bedingt sein. Die maximale Temperatur von 2175 °C am Zentralstab wurde am Ende des Versuches bei maximaler elektrischer Leistung gemessen. Die Unregelmäßigkeiten in der Dampfversorgung können auch der Grund für die unerwartet geringe Oxidation sein.

Die Nachuntersuchungen des Bündels deuten darauf hin, daß die Oxidhaut der Hülle so dünn war, daß sie von dem geschmolzenem nicht oxidierten Zirkaloy herabgespült und aufgelöst wurde. Die Zirkaloyschmelze hat ebenfalls die Oberfläche des Pellets aufgelöst. Die Schmelze ist als zusammenhängender Klumpen im unteren Teil des Bündels erstarrt. Im mittleren Teil des Bündels sind die Pelletreste während des Abkühlens verbröselt und haben sich als feinkörnige Schicht auf dem erstarrten Klumpen angesammelt.

Contents

Introduction

Within the Project of Nuclear Safety (PNS) at the Kernforschungszentrum Karlsruhe (KfK), a comprehensive programm /1/ for the investigation of Severe Fuel Damage (SFD) is scheduled. As part of this programm, out-of-pile experiments are being conducted at the Hauptabteilung Ingenieurtechnik (IT). These experiments provide information on the mechanisms causing damage to PWR fuel rods for temperatures up to 2200°C. These experiments are designed to give information on the integral behaviour of the processes, which are investigated in detail and under well defined conditions in the separate effect tests of the SFD-programm. The out-of-pile experiments will also be used for the assesment of the SFD computer codes to simulate the integral behaviour of the fuel rods under Severe Fuel Damage conditions. In addition, these experiments directly complement integral inpile bundle tests being conducted by EG&G Idaho, Inc., in the Power Burst Facility at the Idaho National Engineering Laboratory /2/.

Earlier experiments have shown that the behavior of fuel rods at high temperatures is strongly dependent on the degree of cladding oxidation. Highly oxidized rods are very brittle and can fragment during operation or during quenching, whereas relatively unoxidized cladding melts, dissolves UO_2, and runs down the rod. The extent of oxidation depends, in part, on the temperature rise rate, which in turn is influenced by the exothermic oxidation process. If the heat of reaction is not removed fast enough, the exponential increase of the reaction with temperature can give rise to a rapid temperature escalation. Therefore, oxidation-induced temperature escalation plays an important role in determining fuel behavior. To investigate the temperature escalation and the processes leading to a turnaround of the escalation, a series of single rod and bundle experiments with fuel rod simulators are being performed.

The results of single rod tests are given in the KfK-report 3507, 3557 and 3567 /3,4,6/. The first bundle test ESBU-1 is described in the KfK-report 3508 /2/. This paper reports on the test conduct and the escalation results of test ESBU-2A. The posttest investigations are given in a later KfK-report.

Temperature Escalation

The oxidation of zirconium in steam is an exothermic reaction which can be expressed as:

$$Zr + 2H_2O \rightarrow ZrO_2 + 2H_2 + 5.86 \times 10^5 \text{ J/mol} \quad (1)$$

In the energy balance, 10.7×10^5 J/mol are gained by the formation of the oxide and 4.81×10^5 J/mol lost by the dissociation of the two moles of H_2O. The energy potential of this reaction is remarkable. The complete oxidation of 10.75 mm zircaloy cladding (1.5 g/cm length) in steam would deliver an energy of 9600 J/cm. Under adiabatic conditions, this energy is sufficient to heat the cladding and fuel to 3700°C, including the melting of both materials.

Zirconium forms a protective layer as it oxidizes. Since the oxidation reaction is controlled by the diffusion of oxygen through the oxide, the reaction rate is inversely proportional to the oxide thickness.

$$\frac{dW}{dt} = \frac{K}{W} \quad (2)$$

where

W = kinetic parameter (oxygen uptake per unit surface area (kg/m^2), metal reacted per unit surface area (kg/m^2), or oxide thickness (m)), and

t = time (s).

The proportionality constant K has been observed to be an Arrhenius function of temperature, so that

$K = A \exp(-B/RT)$

where

A,B = constants to be determined experimentally, and

T = temperature of the cladding (K).

If the heat generated by the reaction is removed from the system so that the cladding temperature remains constant, the rate of reaction declines as 1/W. If the heat is not removed, or is not removed fast enough, the cladding temperature will rise and the exponential dependence of the reaction rate on temperature can dominate the reaction and give rise to a rapid temperature escalation. In this case, the cladding behavior will then be determined by the system boundary conditions (heat removal) and those processes which inherently limit the heat generation in the cladding.

Inherent limitations to the heat gain include: (a) zircaloy consumption, (b) removal of zircaloy from the reaction zone, e.g. molten runoff, (c) steam starvation, and (d) hydrogen blanketing. The heat losses depend on the system temperature, the system configuration, and the available coolant. The modes of heat transport include radiation, convection, and conduction, the relative importance of which depend on the current state of the rod and boundary conditions.

Experiment Facility

The test was performed in the NIELS facility located in the Hauptabteilung Ingenieurtechnik at KfK. Figure 1 shows side and top cross sections of the 3x3 bundle of fuel rod simulators. The simulators conformed as nearly as possible to German PWR dimensions and pitch, using zircaloy cladding of 10.75 mm outer and 9.29 mm inner diameter, UO_2 ring pellets of 9.2 mm outer and 6.1 mm inner diameter, and a tungsten heater element 6.0 mm in diameter. The overall length of the simulators was 400 mm. Figure 3 illustrates the pretest appearance of the bundle.

To simulate the exothermic reaction energy of neighboring rods, a zircaloy shroud was installed around the rod bundle (Figure 3). Radial heat losses were reduced by wrapping the shroud in a ceramic fiber insulation (6 mm) as shown in Figures 5 and 6. Steam was inlet to the bottom of the bundle at 16 locations so that the flow would be evenly distributed across the bundle cross section.

Temperatures were measured by two color pyrometers and NiCr/Ni thermocouples with Inconel sheaths. Four pyrometers were located 255 mm from the bundle bottom, on the sides of the bundle. By removing the middle portion of one of the side rods and making holes in the shroud and insulation, the pyrometers measured temperatures on the central rod surface, two side rod surfaces, and the shroud surface. An additional pyrometer was located 345 mm from the bottom and focused on the center rod (Figure 1). The thermocouple locations are shown in Figure 2. The central rod (5) was instrumented with thermocouples at elevations of 155, 255, and 345 mm. The side rod (4) had thermocouples at elevations of 155 and 345 mm. The shroud was fitted with three thermocouples at the same elevations as the central rod. The insulation was fitted with seven thermocouples as shown in Figure 2, placed at the same elevations as the rods on the outside of the first, third and fifth layers of 1.2 mm thick insulating. Finally, four thermocouples were installed in the steam flow channels, one on the inlet itself, one above the inlet at 50 mm elevation, and two at the steam exit (380 mm elevation), 4 and 15 mm respectively from the shroud wall.

The hottest location in the bundle was anticipated to occur at an elevation of 255 mm. The thermocouples fail around 1300°C and were therefore located away from the hot spot. The thermocouple locations were chosen to provide data on the bundle axial and radial temperature distribution, and the rod circumferential temperature distributions. The shroud thermocouple data provide a check on the pyrometer readings, at temperatures for which both functioned, and the insulation temperatures provide an estimate of the heat losses.

Test Conduct

The original test objective was to heat the rods at a mean rate of about 0.5°C/s. Figure 25 shows the controlled voltage (V), resultant electric current (I), and the calculated resistance (V/I) and electric power (VxI) for all eight rods heated in parallel. The drop in voltage at 57 minutes and the change in voltage rise rate at about 70 minutes was unintentional,

and was caused by failure of the power supply. This resulted in a discontinuity and a change in the temperature rise rate.

A steam flow of about 0.7 g/s was inlet to the bundle beginning at 21 minutes. Figure 46 shows the exit steam temperature at two radial locations, while Figure 47 shows the inlet temperature and the temperature 50 mm above the bundle bottom. The system pressure during the test is shown in Figure 49.

The maximum temperature of 2175°C was measured on the center rod. The experiment was terminated by turning off the electric power at 99 minutes into the test. Then the temperature dropped according to the normal heat losses of the system.

Test Results

The posttest appearance of the insulation, shroud and bundle is shown in Figures 6 to 24. Figures 26-48 present the pyrometer and thermocouple measured temperatures. Figures 26-28 compare pyrometer and thermocouple measured temperatures on the center rod, side rods, and shroud to the electric power. Figures 29-32 shows the temperature measurements by the two color pyrometer with thermocouples at the same position. Figures 33 and 34 combine the temperature measurements of two color pyrometers at the same rod (central rod, fig. 33) and the same elevation (255 mm, fig. 34).

Fig. 35 to 48 shows temperature measurements with thermocouples. Figures 35-37 gives the thermocouple measurements at the 3 measurement elevations of the bundle and insulation. Fig. 38 to 42 give the respective temperatures of the central rod, side rod, shroud and outside of 1.3 and 3.8 mm insulation at the 3 measurement elevations. Fig. 43 to 45 give the temperature at different radial positions in the insulation for each elevation. Fig. 46 and 47 show the steam temperatures at 380 and 50 mm elevation and figure 48 shows the comparison of the exit steam temperatures to temperatures on rods and shroud at nearly the same elevation.

Temperature Escalation Results

There is a steady power increase the first 57 minutes into the test. During this time, the temperature on the center rod reaches about 1200, 1100 and 850°C at the three measuring elevations 255, 155, 345 mm (Figures 35, 36, 37). After the power dip, the temperature decreases and recovers to nearly the same values at about 70 minutes. The mean rate of temperature increase before the power drop is about 0.4°C/sec and this increased to about 0.5°C/sec after 70 minutes.

In the time interval after 70 minutes, a rapid escalation of the temperature occurs. This can be clearly seen at the 255 elavation. Here we have measurements with both two color pyrometers and thermocouples so that temperatures above 1400°C are measured. At the 155 mm elevation only thermocouples are available. At the 345 mm elevation there was one two color pyrometer (on the center rod). Here, no pronounced escalation could be detected (Fig. 26).

The temperature escalation at 255 mm reached a peak of 1500°C at 75 minutes. This can be seen in figures 26 to 34 for the central rod, the side rods, and the shroud. On the central rod, after the peak was reached, a distinct decrease of the temperature for four minutes can be seen.

At the 155 mm elevation, the temperature escalation probably reached higher temperatures. One indication of this is the fact that the thermocouples in the insulation fail much earlier at this elevation compared to the 255 mm elevation (Fig. 36 and 37). Also, at about 75 minutes, the steam temperature at 50 mm elevation inside the channel increases quickly from 400 to 1100°C (Fig. 47). From 80 minutes on, there are temperature peaks at the lower steam distribution tube system (Fig. 47). This appears to be caused by molten droplets falling down on the steam distribution system.

Also, there is a change in the character of the upper end steam temperature (Fig. 46) which reflects a change in the bundle geometry at 75 minutes. We assume that, from this time on, there is some blockage by molten material.

This indication of melting in the bundle at 75 minutes means that the temperature in the region about the 155 mm elevation must have reached the melting temperature of Zircaloy.

The steam was introduced at 21 minutes. One can see a increase of nearly 150°C in the steam temperature measured at 380 mm elevation. This must be connected with the heat transported to the upper part of the bundle by the steam. (The temperature of the thermocouple at 50 mm above bottom went down with the introduction of steam. At this elevation the steam is cooling.)

The oscillation of the steam temperature is probably connected with a variation of steam flow. Checking of the steam production system after the test showed, that a safety valve opened much to early. We assume that in the test this valve was opening in a periodic way, reducing the steam flow through the bundle.

Due to the higher initial temperature, the escalation at the 255 mm elevation occured first. Then, the temperature at the 155 mm elevation is assumed to escalate. Due to the reduced steam supply, the oxygen was consumed in the lower region. Therefore, in the 255 mm elevation, not enough steam was available and the escalation was stopped. At 345 mm the temperature was the lowest from the beginning. Therefore no escalation could develop at all.

As the test continued, the temperature on the center rod reached a peak of 2175°C. Temperatures on the side rods and shroud also reached peaks of almost 2100°C at the same time. 2100°C is sufficient to melt α-Zr(O) and cause substantial dissolution of UO_2 by molten zircaloy that comes in contact with it, depending on the oxide content of the zircaloy /7/. As the posttest appearance of the bundle shows, all of the cladding and some fuel over a substantial part of the bundle had melted and run down, refreezing in a lump near the bottom of the bundle.

Axial Temperature Distribution

The axial temperature distribution within the bundle can be seen in Figure 26, comparing the center rod temperatures at 255 and 345 mm. In addition, the axial temperature distribution can be seen in Figures 38-42 which show the thermocouple readings from each elevation for the center rod, side rod, shroud, and two locatins in the insulation. The temperature at 255 mm was always the hottest. Steam superheating as it flowed through the bundle certainly caused the temperatures to shift upwards axially.

Figures 41 and 42 show that, beginning at 70 minutes, the temperature in the insulation at 155 mm increased rapidly until, at 75 minutes, it was nearly equal to the temperature at 255 mm. This is probably the result of relocation of molten material to the bottom of the bundle and an almost complete blockage of the bundle. Thus, the melt was most likely in contact with the shroud wall at this point, raising the insulation temperature.

Radial Temperature Distribution

The radial temperature distribution at 255 mm is shown in Figures 27, 28 and 34. Less than 100°C separated the side rods from the peak temperature on the center rod for most of the high temperature phase of the test. The shroud temperature was, at most, 200°C less than the center rod, and basically the shroud temperature followed the heater rod temperatures.

The temperatures measured with thermocouples for the center rod, side rod, shroud, and locations within the insulation are shown in Figures 35-37 for the 345, 155, and 255 mm elevations.

The thermocouple measurements at all three elevations show that, with the introduction of the steam at 21 minutes, the temperature of the central rod goes up slightly and the temperature of the shroud goes down. The temperature of the side rod shows no significant change with the introduction of steam.

As the bundle temperature increases, there is the tendency for the difference between center rod and shroud temperature to decrease (from ca. 300 to 100°C). On the other hand, the temperature drop in the insulation increases signifacantly (from ca. 50 to over 400°C for the 255 mm elevation), since with higher temperatures the losses become higher.

Steam Temperatures

Steam temperatures were measured at the inlet, 50 mm above the inlet, and 380 mm above the inlet (almost bundle exit) (Figures 46-48). At the upper location two thermocouples were installed, 4 and 15 mm from the shroud wall. During the first 21 minutes, the steam thermocouple located in the space between outer rods and shroud (temperature curve marked with 4 mm in Fig. 48) gave measurements between the values for the shroud and outer rods. The thermocouple located between outer and inner rod (85 mm in Fig. 48), during this time, gave values between those of the outer rod and center rod. Through the early part of the test (up to 50 minutes), the steam temperature was between the rod and shroud temperatures of nearly the same elevation (Figure 48). Later in the test, as radiation dominated the heat transfer, the steam temperatures fell below the shroud temperatures.

As discussed earlier, the steam thermocouples at the inlet and 50 mm appear to have been influenced by melt. In particular, the 50 mm thermocouple indicates a melt temperature of nearly 1400°C at 92 minutes. The reading also indicates that the temperature declined rapidly after 92 minutes, although the power was not shut off until 99 minutes. However, this could simply be the result of the thermocouple failing. In any event, the initial temperature rise corresponds very well with other temperature indications of rod failure and melting.

Posttest Appearance

The posttest appearance of the bundle before removing the insulation is shown in Figure 6. The insulation and shroud were still intact following the test. However, both were severely embrittled, as the removal of the insulation from the shroud showed (Figure 7). The insulation, originally a flexible mat, broke into many pieces (Figure 7 + 21). Even though the insulation was carefully removed, pieces of the shroud broke off (Figures 7). Powdery rubble was found below the test rig during disassembly of the bundle (Figure 8). The shroud was severely oxidized over the center region of the bundle and broke away in several places, revealing the fuel rod simulators (Figure 9). Figures 10 and 11 show closeups of the remaining upper and lower shroud, respectively.

Figure 12 shows the fuel rod simulators after removal of the shroud. The cladding from all nine rods melted in the center region of the bundle, liquefied some fuel, flowed down the rods, and froze in a solid mass near the bottom of the bundle. The frozen material substantially blocked the coolant flow channels. The shroud adhered to the refrozen mass. A large amount of powdery rubble, probably fuel fractured during cooldown, was found on top of the blockage (Figures 13-15).

Figure 16 shows the appearance of the bundle after removal of the rubble. The upper end of the bundle contains intact but oxidized zircaloy cladding. Below this region (Figure 17) the remains of fuel pellets that stuck to the tungsten heater rod can be seen. Below the blockage (Figure 18) the cladding appeares metallic near the steam inlet, changing to oxidized zircaloy near the lower end of the blockage.

The lower part of the refrozen melt (Figure 18) shows poor wetting of the solid surface, as indicated by the large wetting angles and small contact areas. Melt viscosity, oxygen content, and relatively cold fuel rod simulators probably influenced the refreezing behavior in this region.

The upper surface of the blockage (Figures 19 and 20) has a smooth surface and wet the remaining simulators rather well (small wetting angle and large contact surface). This indicates that the melt interacted with the oxidized fuel rod simulators and steam. The composition of the melt and these interactions will be the primary subject of the posttest examination.

Conclusion

Five important modes of material behavior occurred during test ESBU-2A: (a) temperature escalation due to the zircaloy/steam reaction, (b) zircaloy melting, fuel liquefaction, and runoff, (c) melt interaction with steam, (d) melt interaction with oxidized zircaloy, and (e) fuel fracturing. The temperature escalation that occurred was not of the magnitude seen in other tests /2/. It was concluded from the combination of different thermocouple results, that the escaltion to the highest temperatures occured in the lower region of the bundle. The initial melting and the dissolution of UO_2 occured with this escalation. Due to a failure in the steam production system, steam starvation may have occured in the upper part thus explaining the moderate escalation at the 255 mm elevation. The final maximum measured temperature of 2175°C in this test appears to be the result of electric heating.

Acknowledgement

The authors would particularly like to thank Mr. Albiez for the data processing and graph preparation, Mr. Brand for taking the photographs and Mrs. Ivanitsch for her careful typing of the manuscript. We thank Mr. B. Buescher for proof reading and discussions. We are grateful to Mr. Frank Panisko for arranging the delivery of the zircaloy for the shroud.

References

1. A. Fiege
"Severe Fuel Damage Research in Germany - A Review of the KfK/PNS Program,"
International Meeting on Light Water Reactor Severe Accident Evaluation, Cambridge, Massachusetts, USA,
August 28 - September 1, 1983

2. S. Hagen, S.O. Peck
Temperature Escalation in PWR Fuel Rod Bundles due to the Zircaloy/Steam Reaction: Bundle Test ESBU-1, Test Result Report,
KfK-Report 3508, 1983

3. S. Hagen, H. Malauschek, K.P. Wallenfels, S.O. Peck
Temperature Escalation in PWR Fuel Rod Simulators due to the Zircaloy/Steam Reaction: Tests ESSI 1-3, Test Results Report,
KfK-3507, 1983

4. S. Hagen, H. Malauschek, K.P. Wallenfels, S.O. Peck
Temperature Escalation in PWR Fuel Rod Simulators due to the Zircaloy/Steam Reaction: Tests ESSI 4-11, Test Results Report,
KfK-3557, 1983

5. P.E. McDonald, G.P. Marino
Power Burst Facility Severe Fuel Damage Test Program,
EG&G Idaho, Inc., EGG-J-04282, October 1982

6. S. Hagen
Out-of-pile Experiments on the High Temperature Behaviour of Zry-4 Clad Fuel Rods,
KfK-Report 3567, 1983

List of Figures

Fig. 16: Posttest appearance of the ESBU-2A bundle after removal of the rubble.

Fig. 17: Close-up of the upper portion of the ESBU-2A bundle.

Fig. 18: Close-up of the lower portion of the ESBU-2A bundle.

Fig. 19: Enlarged view of the ESBU-2A blocked region from above: Two orientations.

Fig. 20: Enlarged view of the ESBU-2A blocked region from above: Two orientations.

Fig. 21: Posttest appearance of the ESBU-2A insulation after removal.

Fig. 22: Posttest appearance of the ESBU-2A shroud after removal.

Fig. 23: Close-up of the ESBU-2A shroud showing the outer surfaces.

Fig. 24: Close-up of the ESBU-2A shroud showing the inner surfaces.

Fig. 25: Voltage V, current I, electric power E and resistance R for test ESBU-2A.

Fig. 26: Temperatures on the central rod (5) at the 255 (II) and 345 mm (III) elevations compared to the electric power (E).

Fig. 27: Temperatures at the 255 mm midplane on the central rod (5). Side rods (4+8) and shroud (s) compared to the electric power (E).

Fig. 28: Temperatures at the 255 mm midplane on the central rod (5) and the shroud (s) in comparison to the electric power (E).

Fig. 29: Temperatures measured by thermocouple and two color pyrometer on central rod (5) at 255 mm elevation (II).

Fig. 30: Temperatures measured by thermocouple and two color pyrometer on central rod (5) at 345 mm elevation (III).

Fig. 31: Temperatures measured by two color pyrometer at 255 mm elevation (II) on the side rods (4+8) compared to thermocouple measurements on the shroud (s).

Fig. 32: Tmeperatures measured by thermocouple and two color pyrometer on the shroud A1 the 255 mm elevation (II).

Fig. 33: Temperatures measured by two color pyrometers on the central rod (5) at the 255 mm (II) and the 345 mm elevation (III).

Fig. 34: Temperatures measured by two color pyrometers at the 255 mm midplane (II) on the central rod (5), two side rods (4+8) and the shroud (s).

Fig. 35: Temperatures at the 345 mm elevation on central rod (5), side rod (4), shroud (s) and 1.3 mm (I1) and 3.8 mm (I3) into the fiber ceramic insulation.

Fig. 36: Temperatures at the 155 mm elevation on central rod (5), side rod (4), shroud (s) and 1.3 mm (I1) and 3.8 mm (I3) into the fiber ceramic insulation.

Fig. 37: Temperatures at the 255 mm (II) elevation on central rod (5), shroud (s) and 1.3 mm (I1), 3.8 mm (I3) and 6.4 mm (I5) into the fiber ceramic insulation.

Fig. 38: Temperatures on the central rod (5) at 155 mm (I), 255 mm (II) and 345 mm (III) elevations.

Fig. 39: Temperatures on the side rod (4) at the 155 mm (I) and 345 mm (III) elevations.

Fig. 40: Temperatures on the shroud (s) at the 155 mm (I), 255 mm (II) and 345 mm (III) elevations.

Fig. 41: Temperatures in the insulation 1.3 mm into the fiber ceramic at the 155 mm (I), 255 mm (II) and 345 mm (III) elevations.

Fig. 42: Temperatures in the insulation 3.8 mm into the fiber ceramic at the 155 mm (I), 255 mm (II) and 345 mm (III) elevations.

Fig. 43: Temperatures in the insulation at the 155 mm (I) elevation 1.3 mm (I1) and 3.8 mm (I3) into the fiber ceramic.

Fig. 44: Temperatures in the insulation at the 255 mm (II) elevation 1.3 mm (I1) and 3.8 mm (I3) and 6.4 mm (I5) into the fiber ceramic.

Fig. 45: Temperatures in the insulation at the 345 mm (III) elevation 1.3 mm (I1) and 3.8 mm (I3) into the fiber ceramic.

Fig. 46: Steam temperatures at 380 mm above the lower end of the cladding at a 4 mm and 15 mm radial distance from the shroud.

Fig. 47: Steam temperatures at 50 mm above the lower end of the cladding at a 15 mm radial distance from the shroud and temperature at the steam distribution system (D).

Fig. 48: Steam temperature at 380 mm above the lower end of the cladding at a 4 mm and a 15 mm radial distance from the shroud compared to the temperature on the central rod (5), side rod (4) and shroud (S) at 345 mm.

Fig. 49: Pressure in the test vessel for test ESBU-2A.

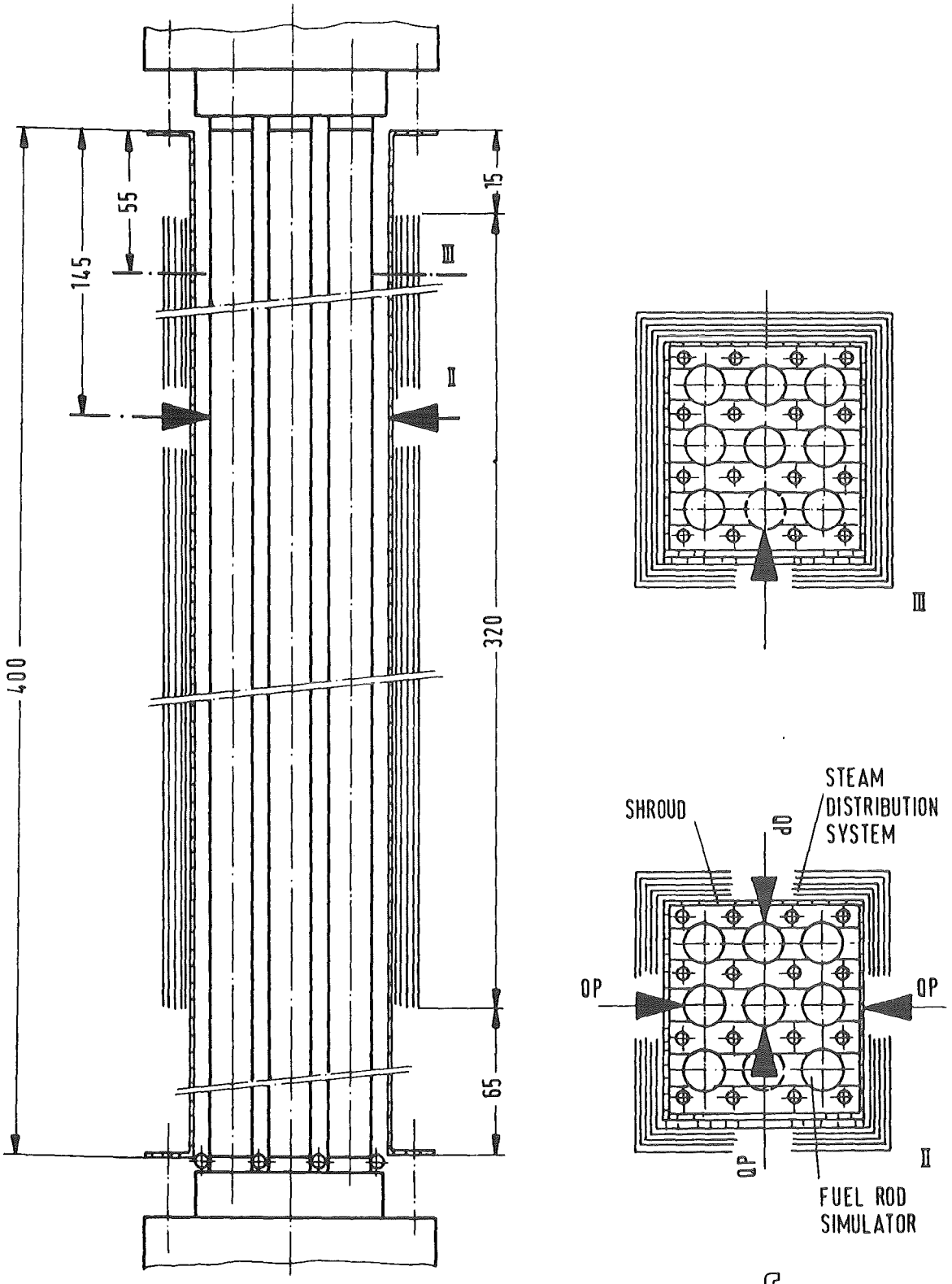

FIGURE 1: ESBU-2A AXIAL AND RADIAL CROSS SECTIONS AND THE LOCATIONS OF THE TWO-COLOR PYROMETERS

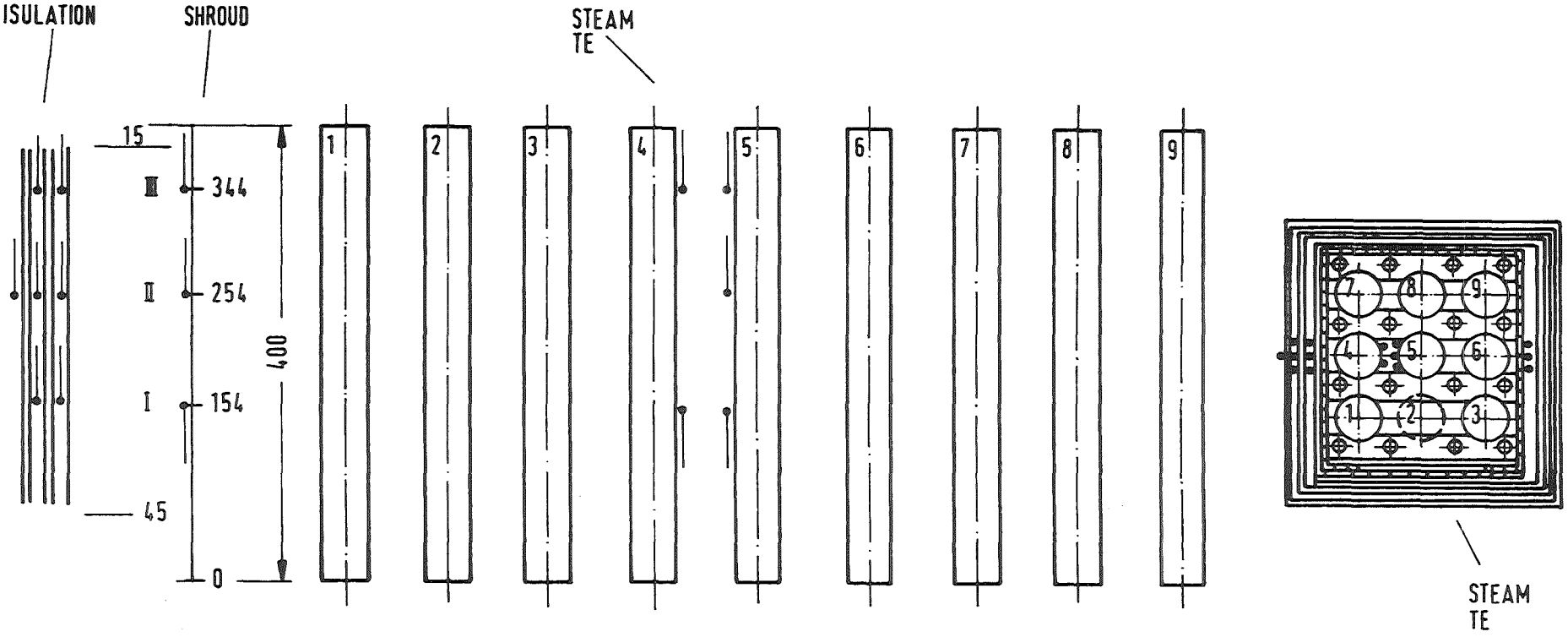

FIGURE 2: AXIAL AND RADIAL POSITIONS OF THE THERMOCOUPLES OF TEST ESBU-2A

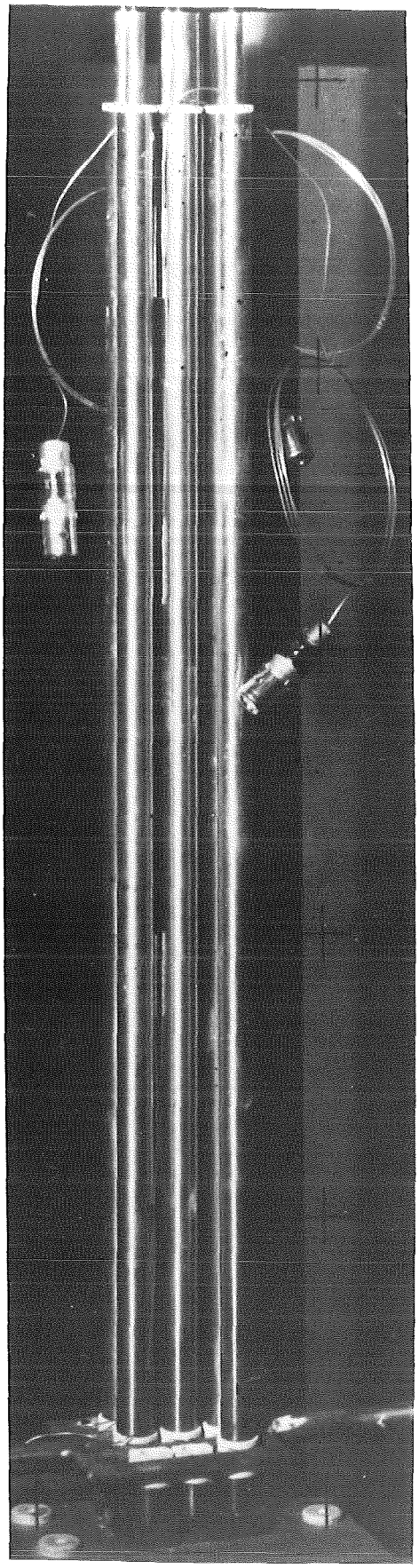

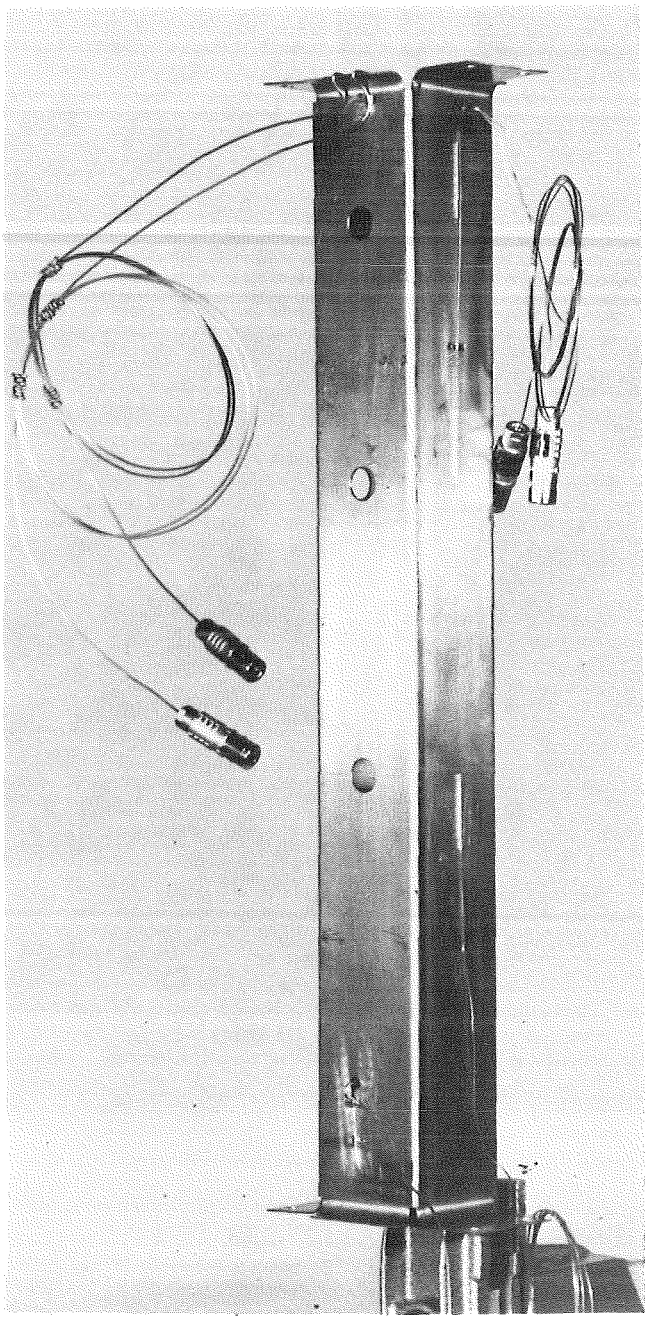

FIGURE 3: PRETEST APPEARANCE OF THE ESBU-2A BUNDLE AND SHROUD

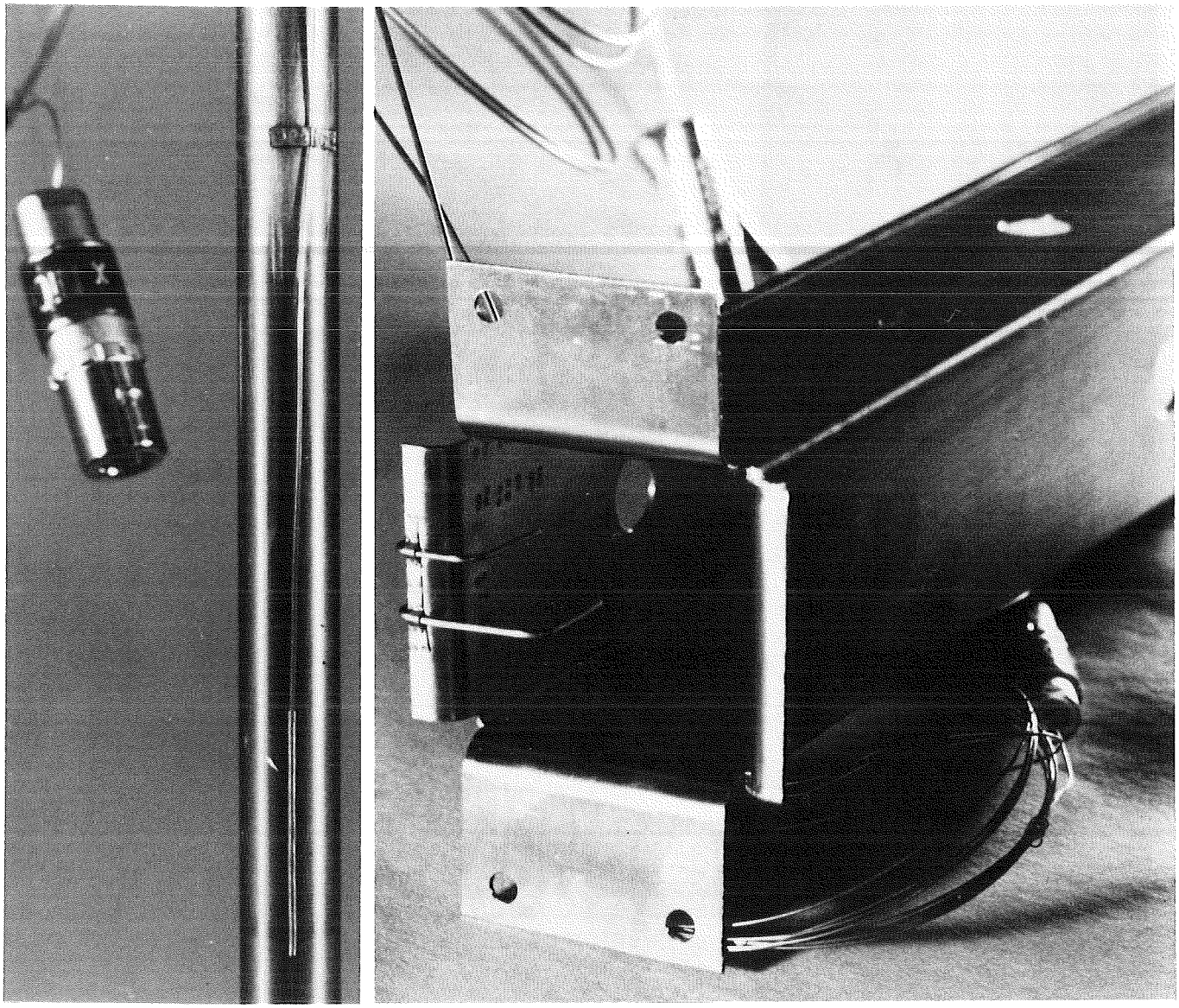

FIGURE 4: ESBU-2A ROD AND SHROUD THERMOCOUPLES

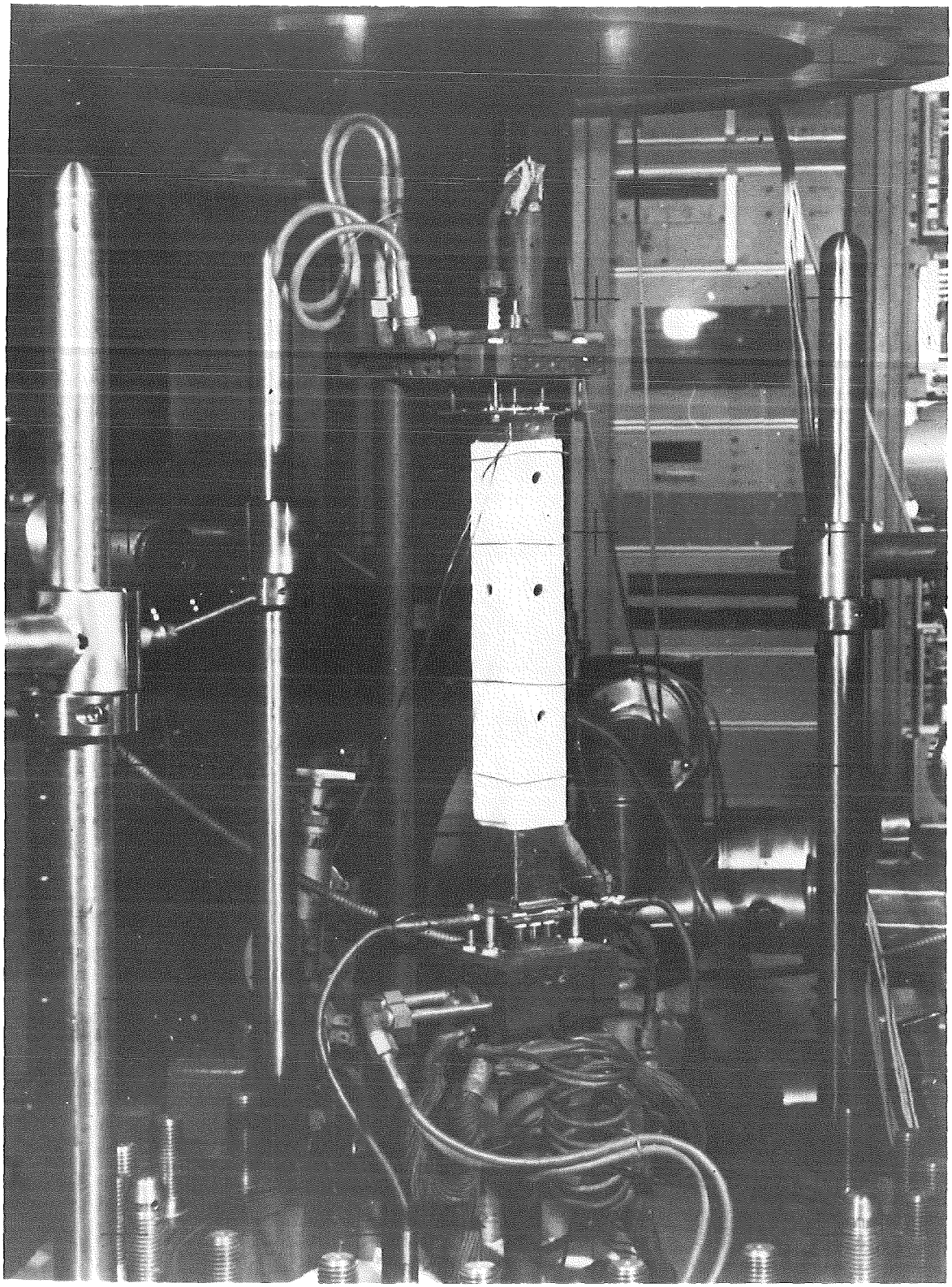

FIGURE 5: GENERAL VIEW OF ESBU-2A WITH ELECTRICAL CONNECTIONS AND TWO-COLOR PYROMETERS

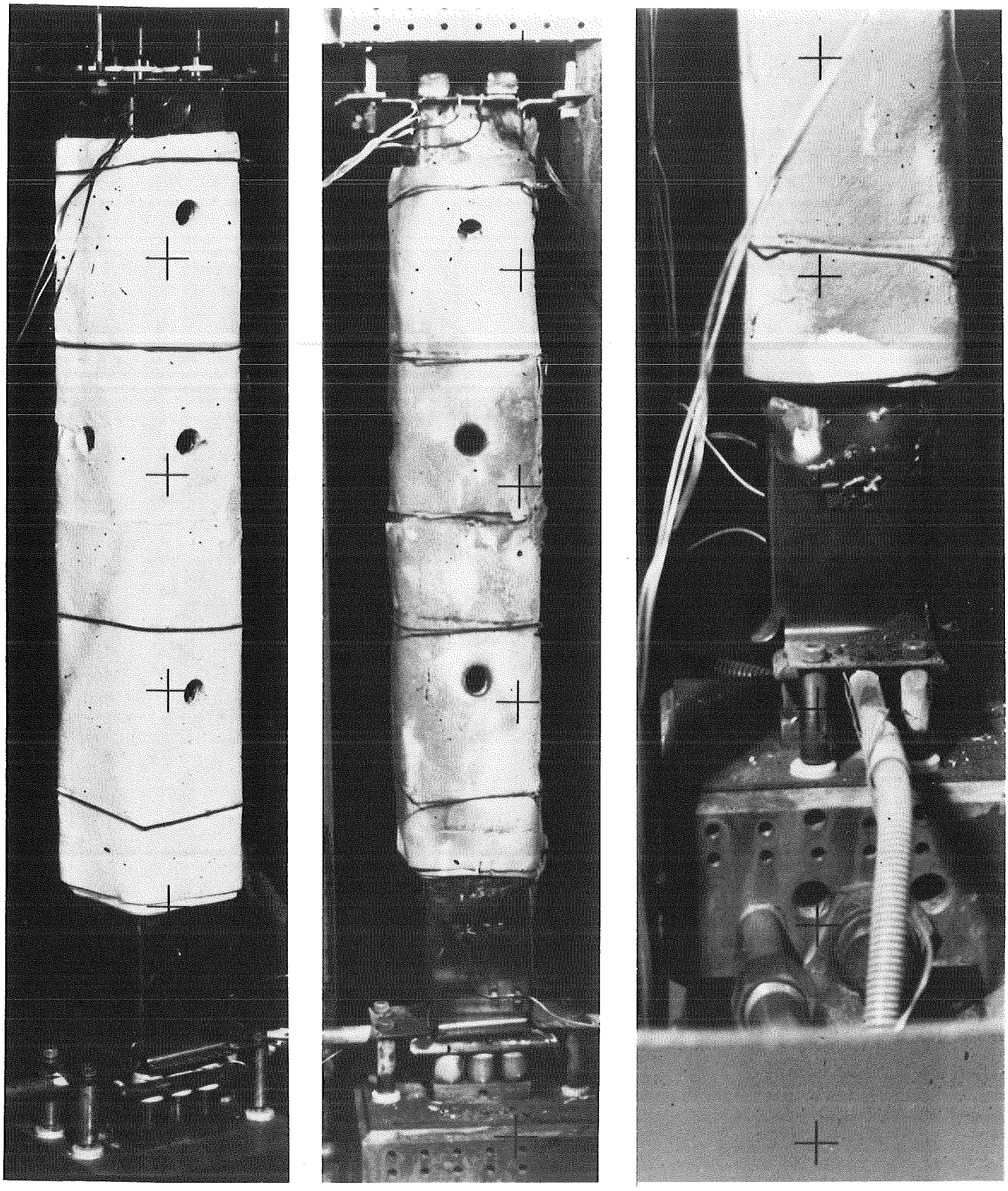

FIGURE 6: PRE-AND POSTTEST APPEARANCE OF ESBU-2A WITH INSULATION. NOTE POWDERY RUBBLE IN THE THIRD PICTURE

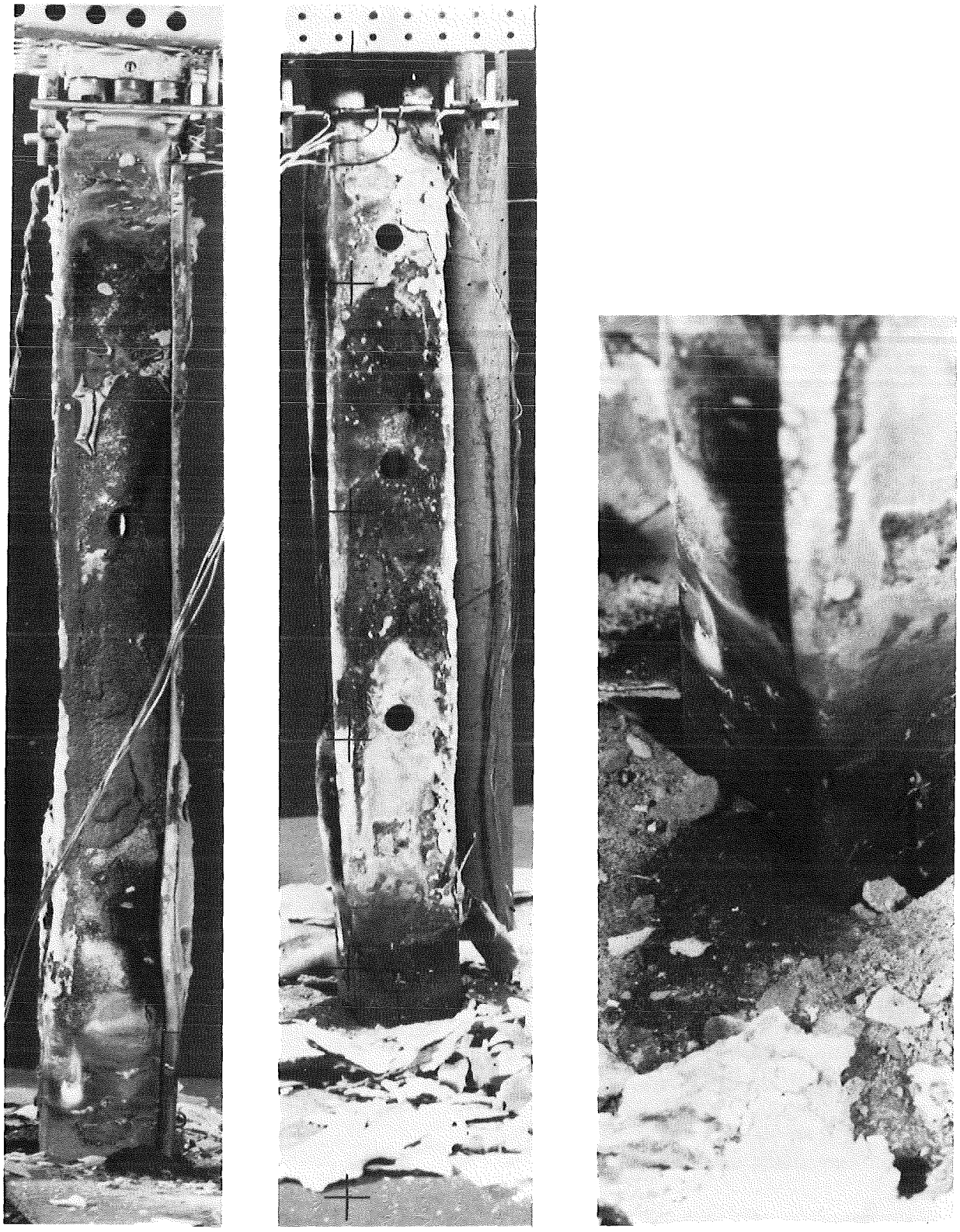

FIGURE 7: POSTTEST APPEARANCE OF THE ESBU-2A SHROUD AFTER REMOVAL OF THE INSULATION

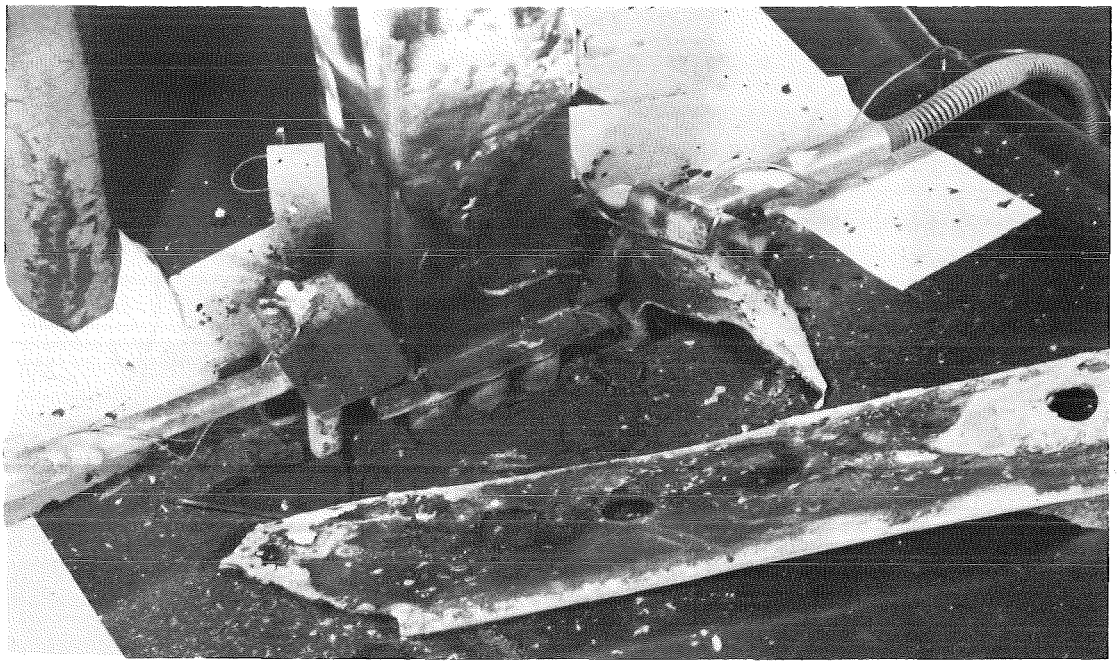

FIGURE 8: POWDERY RUBBLE FOUND DURING DISASSEMBLY OF ESBU-2A

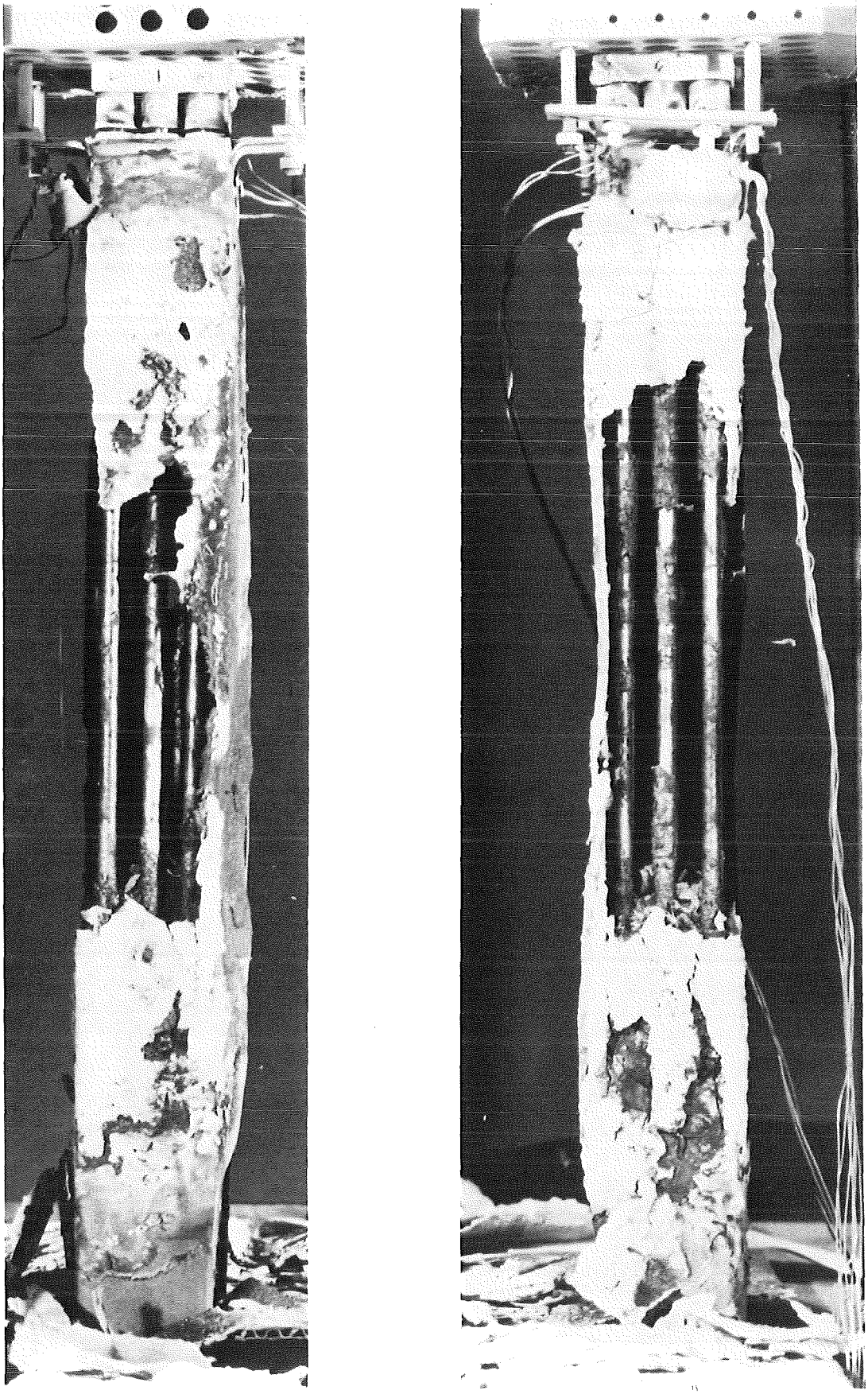

FIGURE 9: PARTIAL DISASSEMBLY OF THE HIGHLY EMBRITTLED ESBU-2A SHROUD

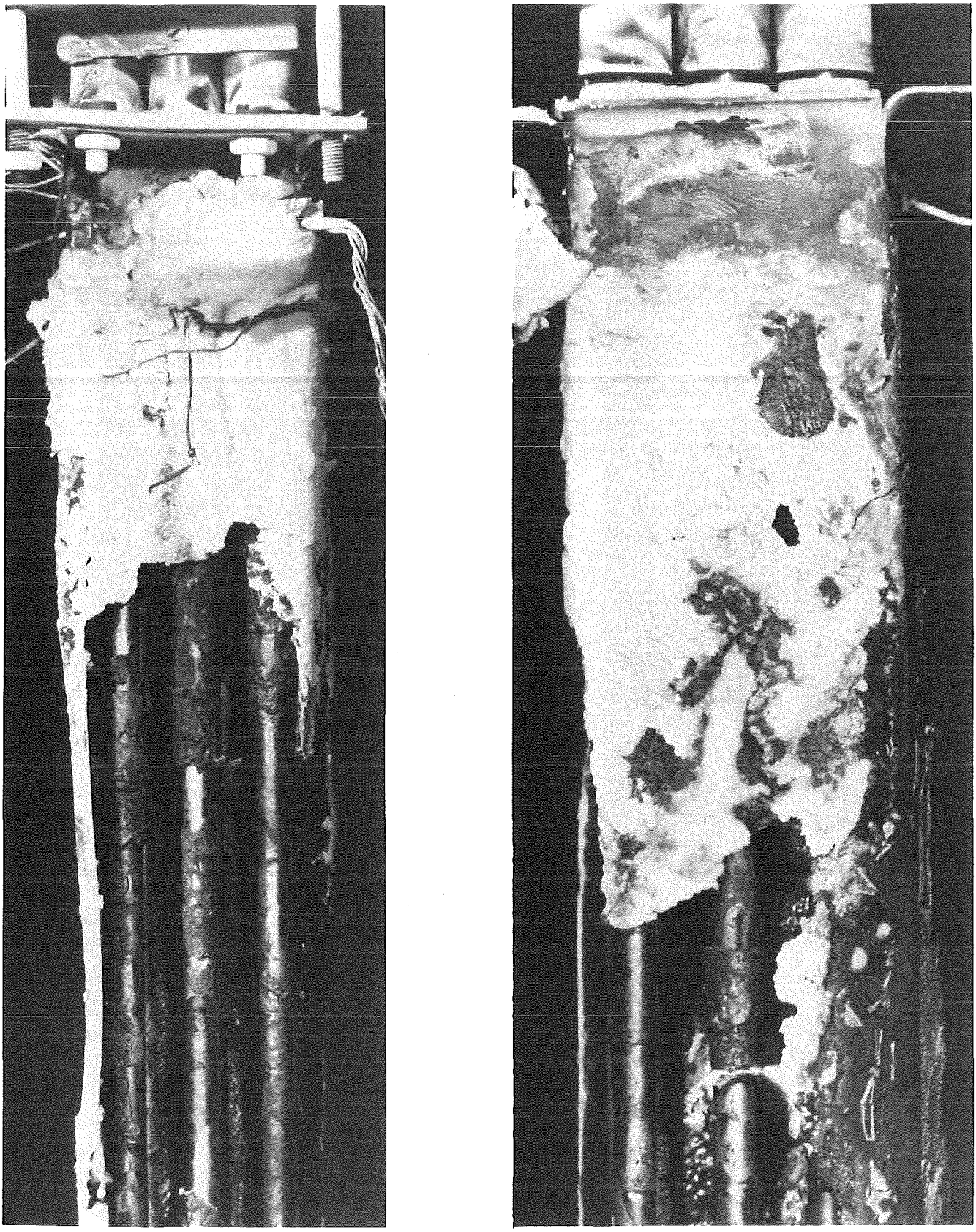

FIGURE 10: CLOSE-UP OF THE UPPER PORTION OF THE ESBU-2A SHROUD

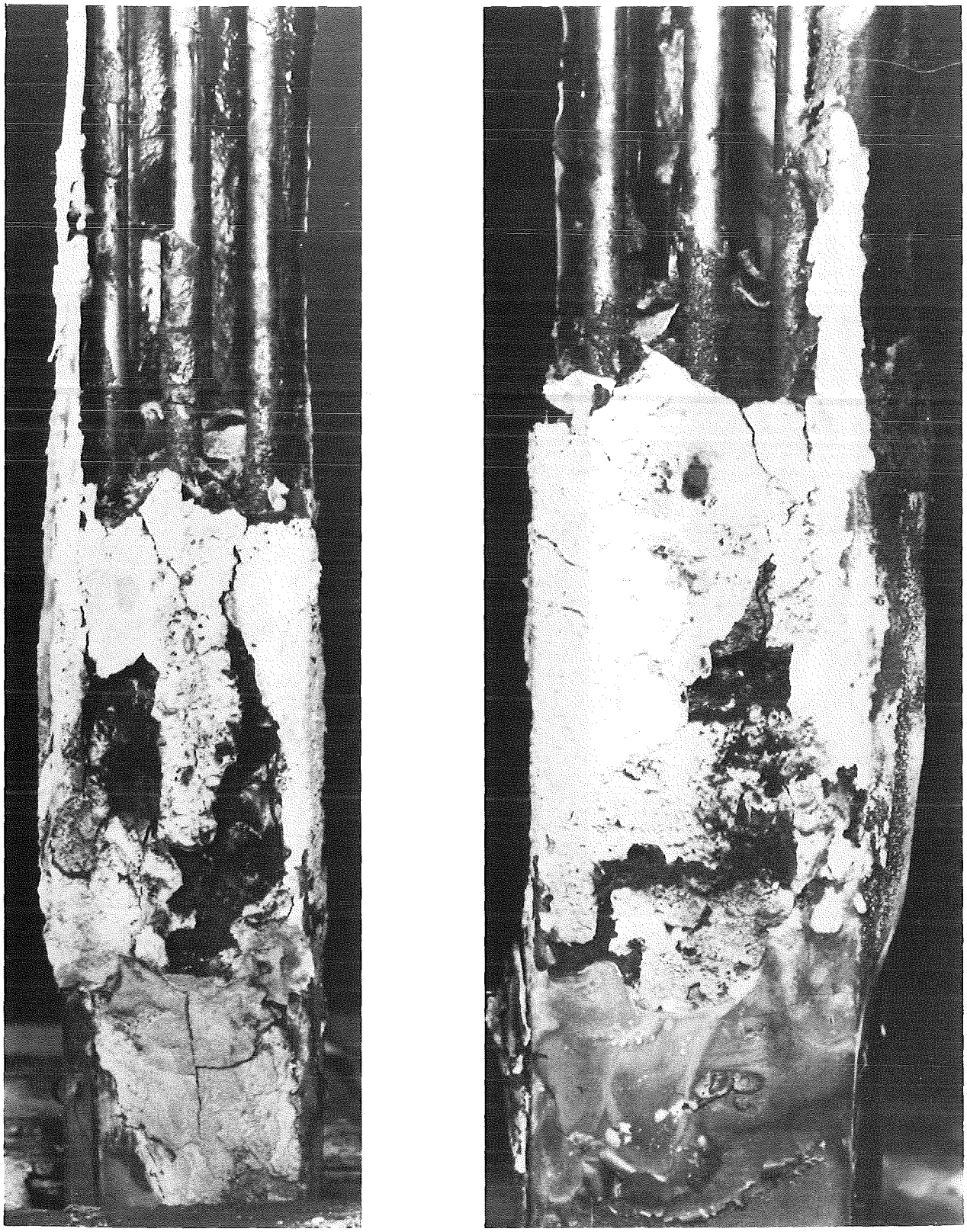

FIGURE 11: CLOSE-UP OF THE LOWER PORTION OF THE ESBU-2A BUNDLE

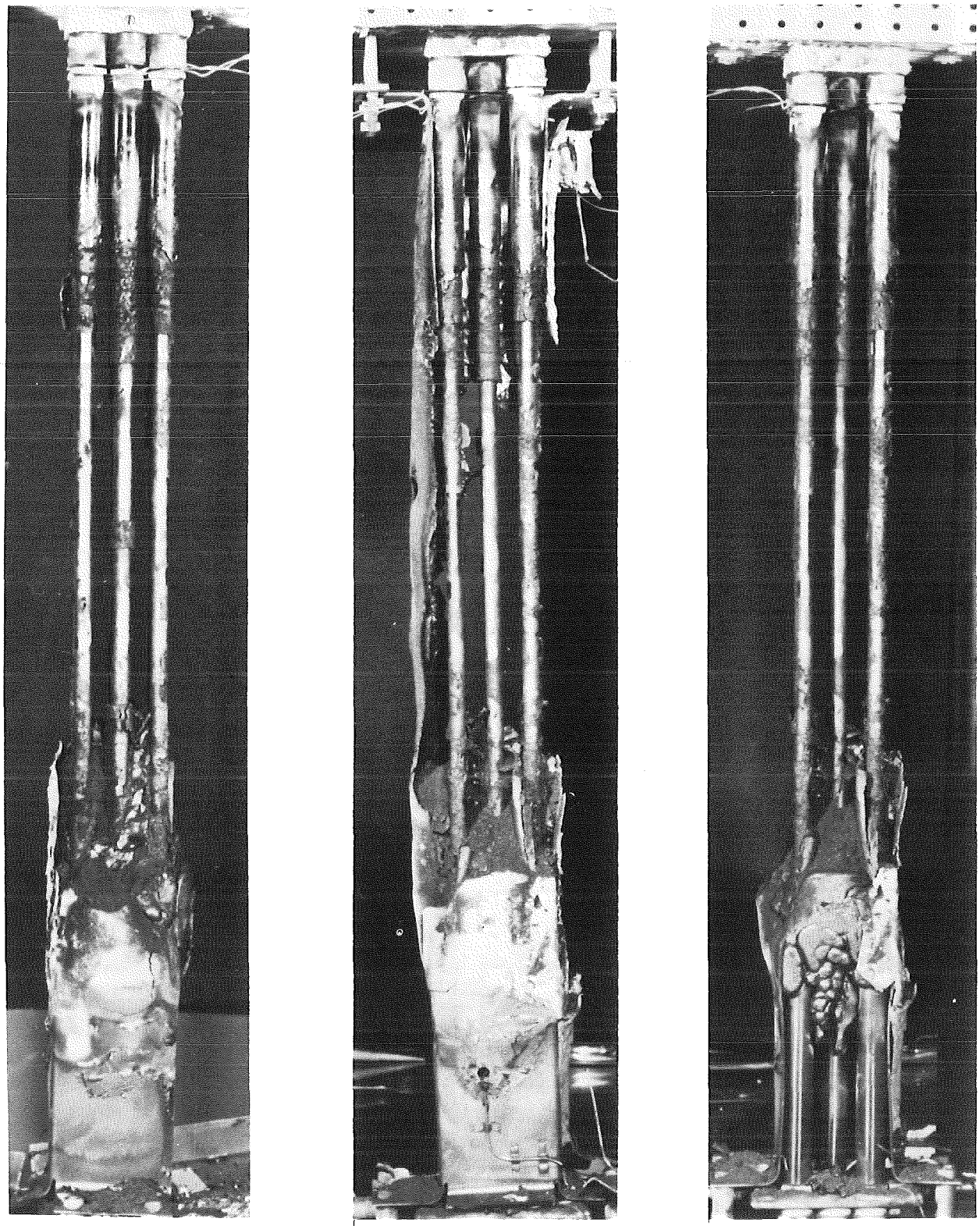

FIGURE 12: POSTTEST APPEARANCE OF THE ESBU-2A BUNDLE

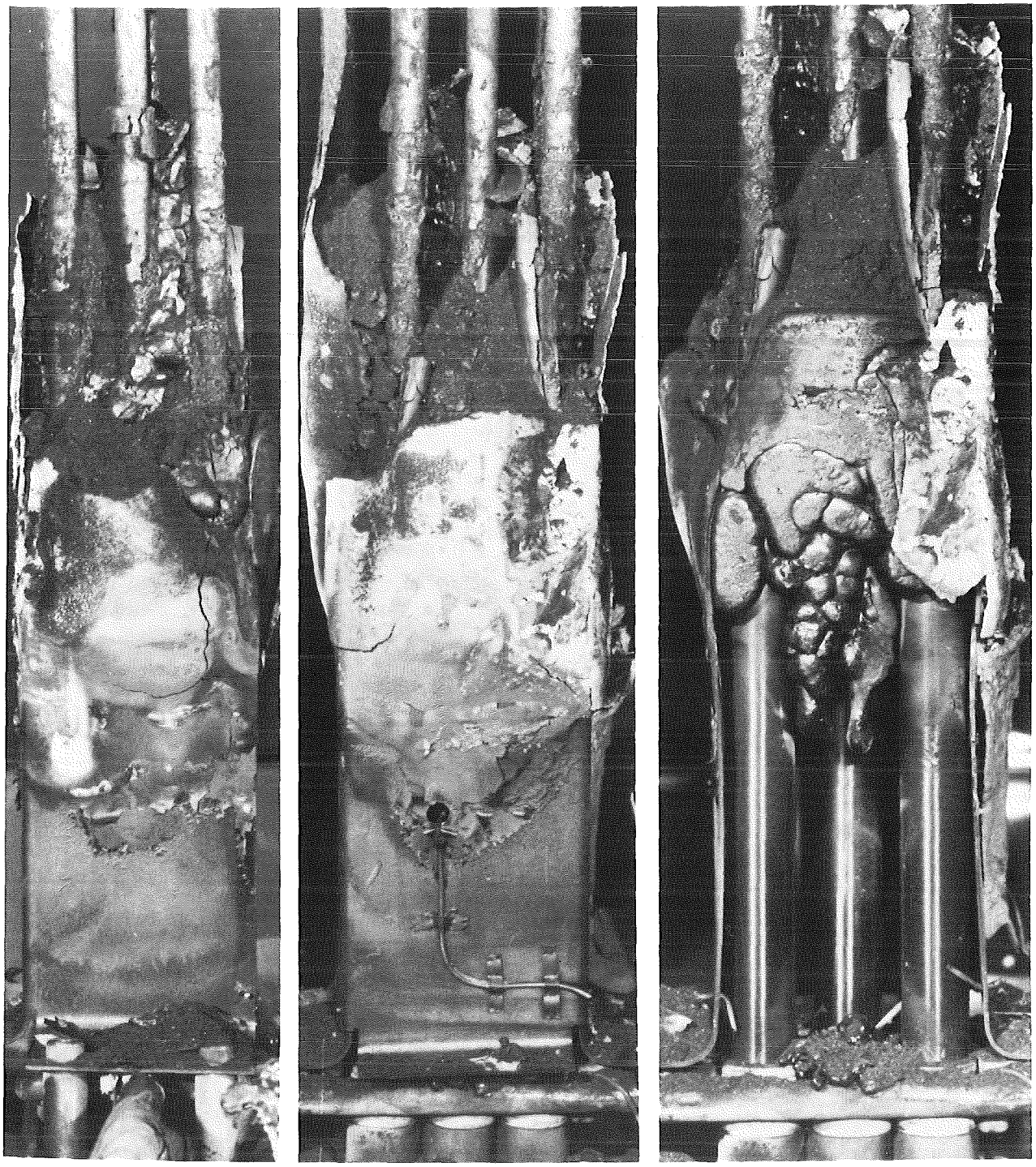

FIGURE 13: CLOSE-UP OF THE BLOCKED REGION OF ESBU-2A INCLUDING POWDERY RUBBLE

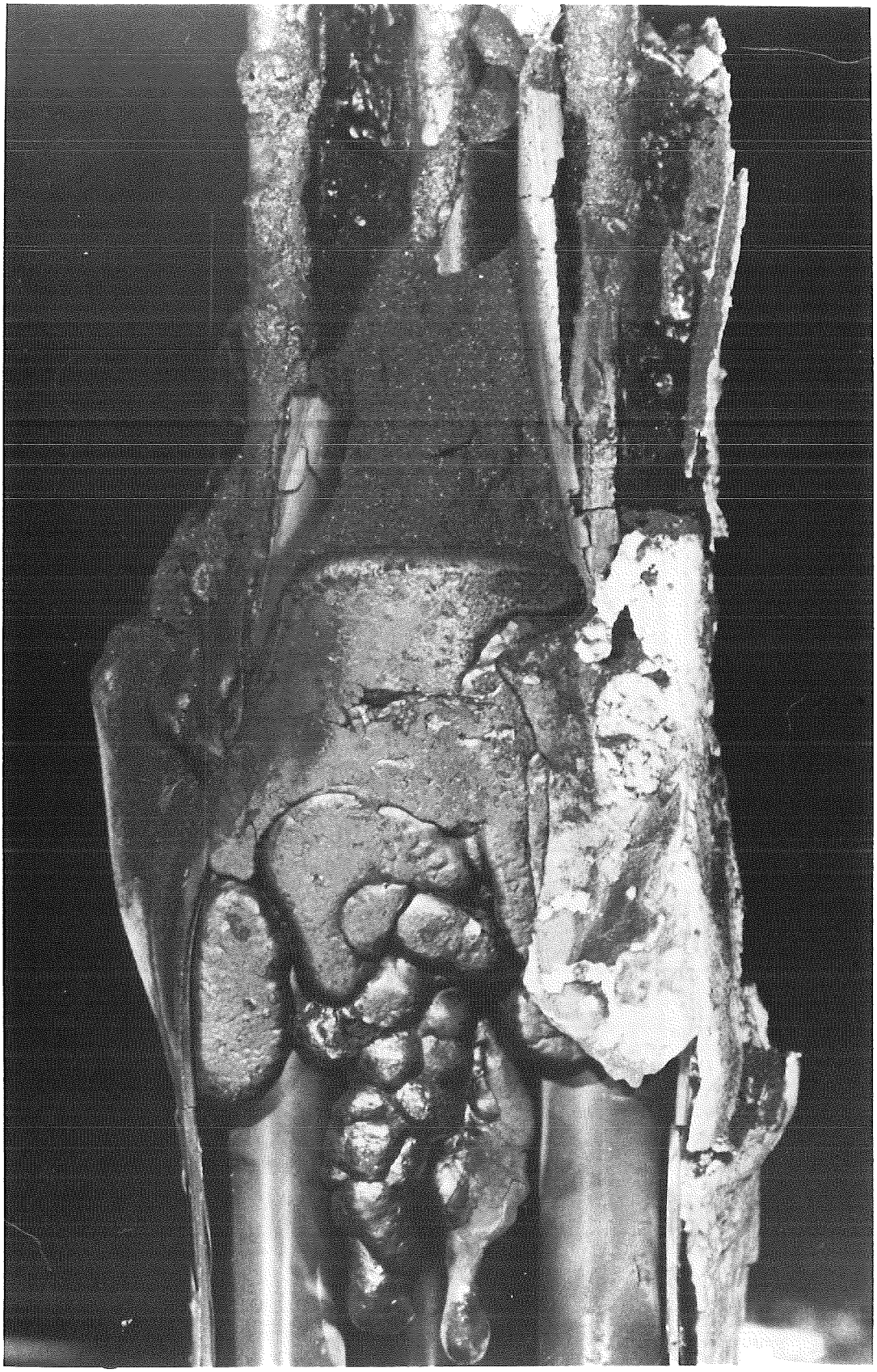

FIGURE 14: ENLARGEMENT OF THE REFROZEN MELT AND POWDERY RUBBLE FROM ESBU-2A

FIGURE 15: ENLARGEMENT OF THE RUBBLE FOUND ABOVE THE REFOZEN MELT IN ESBU-2A

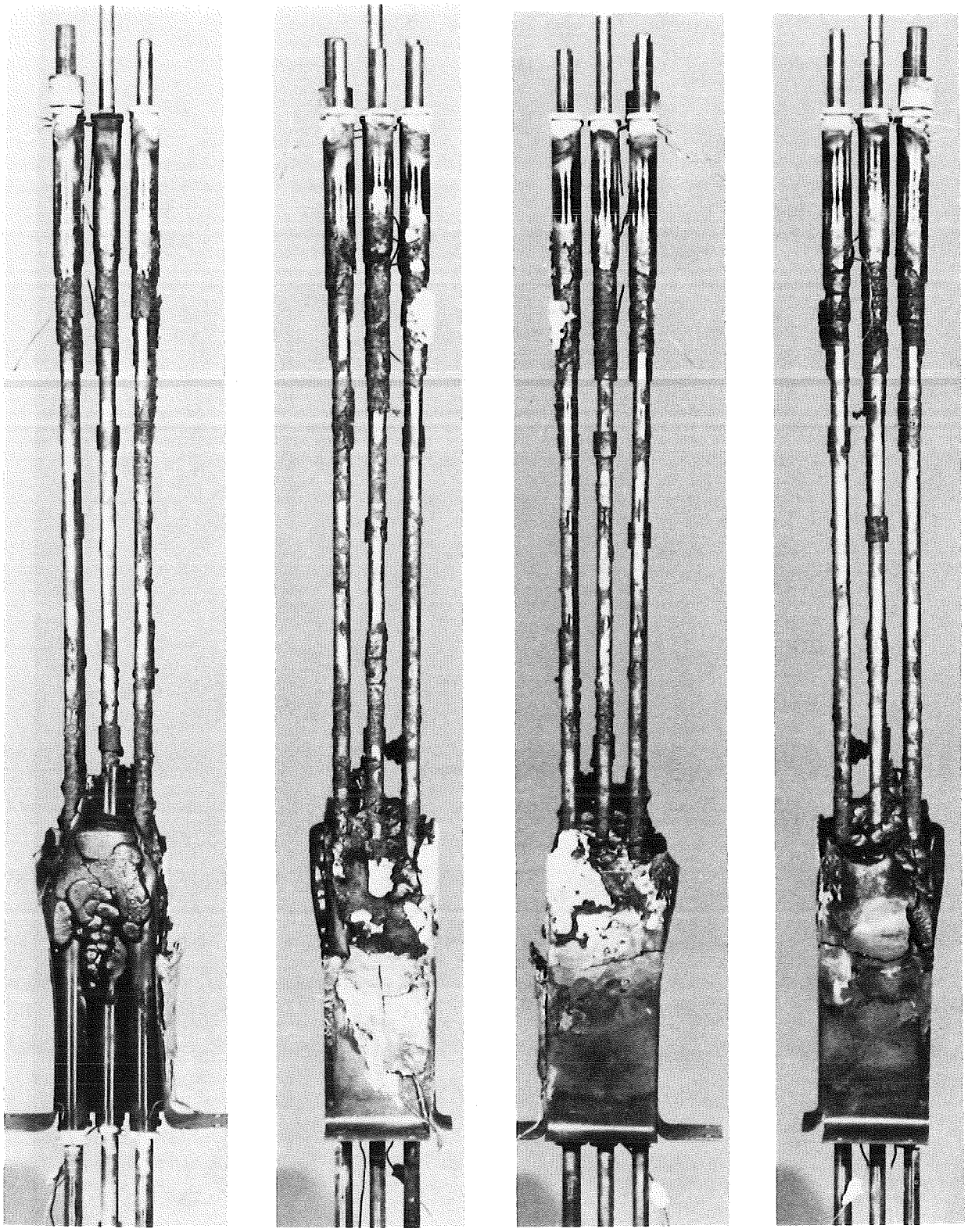

FIGURE 16: POSTTEST APPEARANCE OF THE ESBU-2A BUNDLE AFTER REMOVAL OF THE RUBBLE

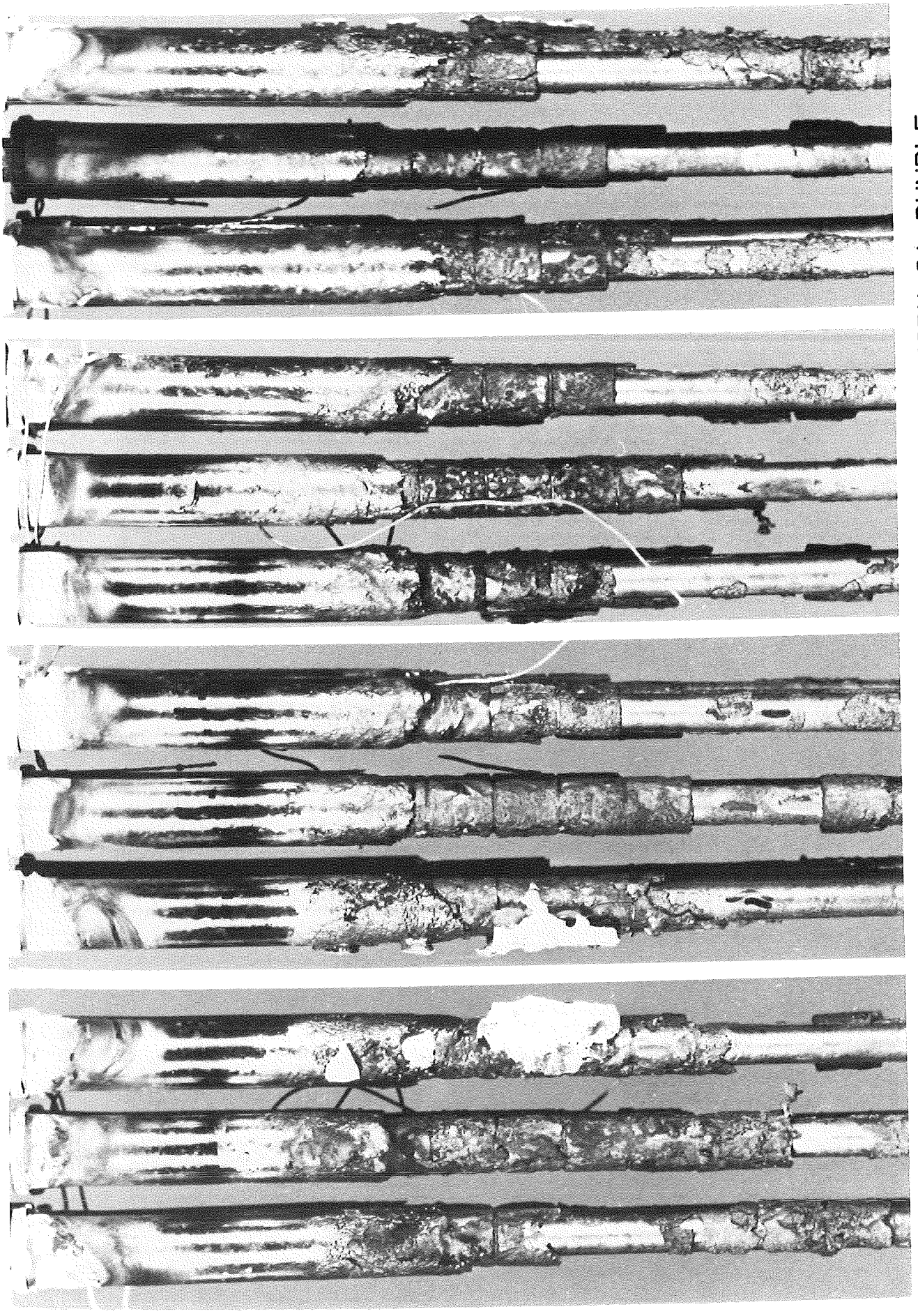

FIGURE 17: CLOSE-UP OF THE UPPER PORTION OF THE ESBU-2A BUNDLE

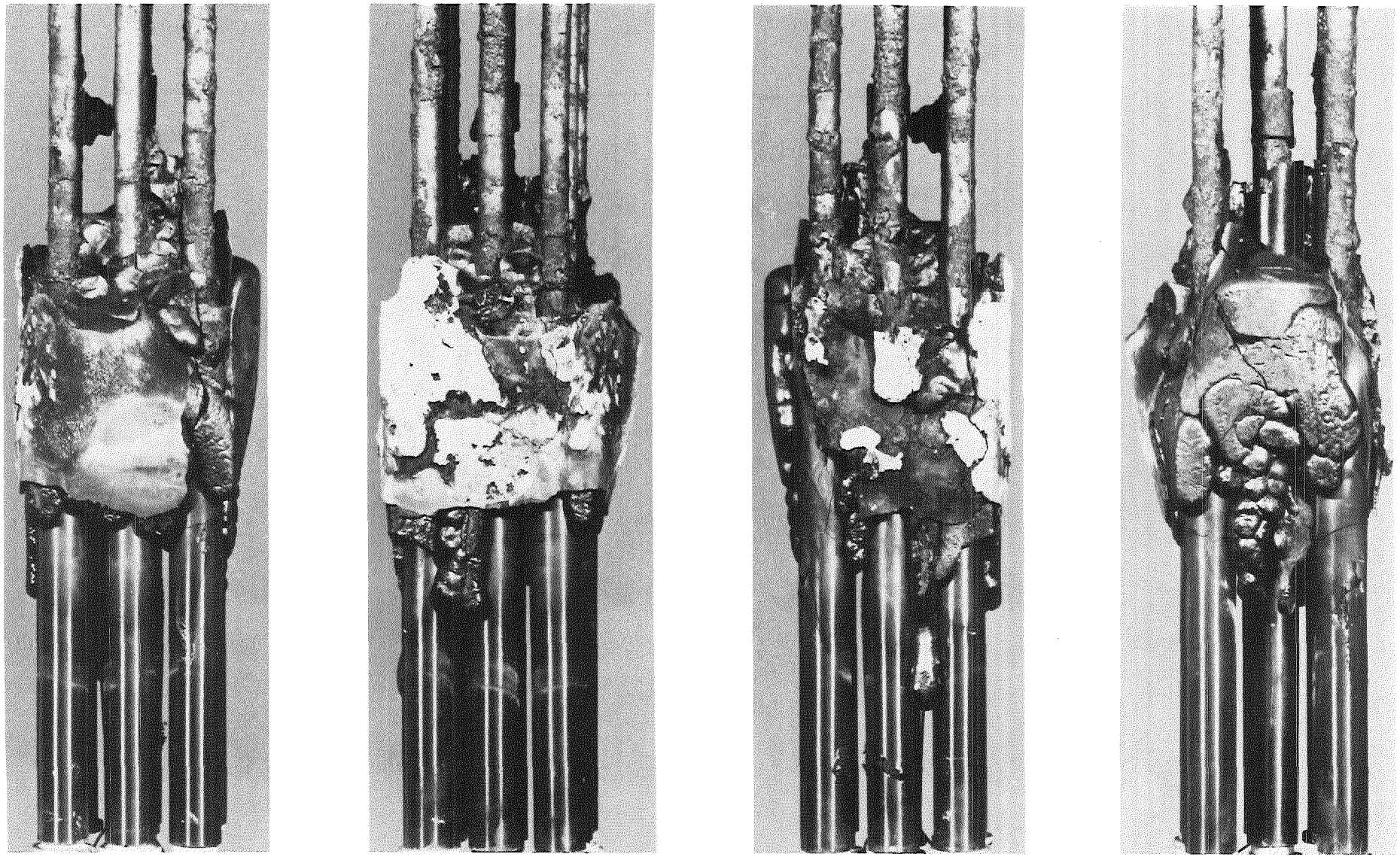

FIGURE 18: CLOSE-UP OF THE LOWER PORTION OF THE ESBU-2A BUNDLE

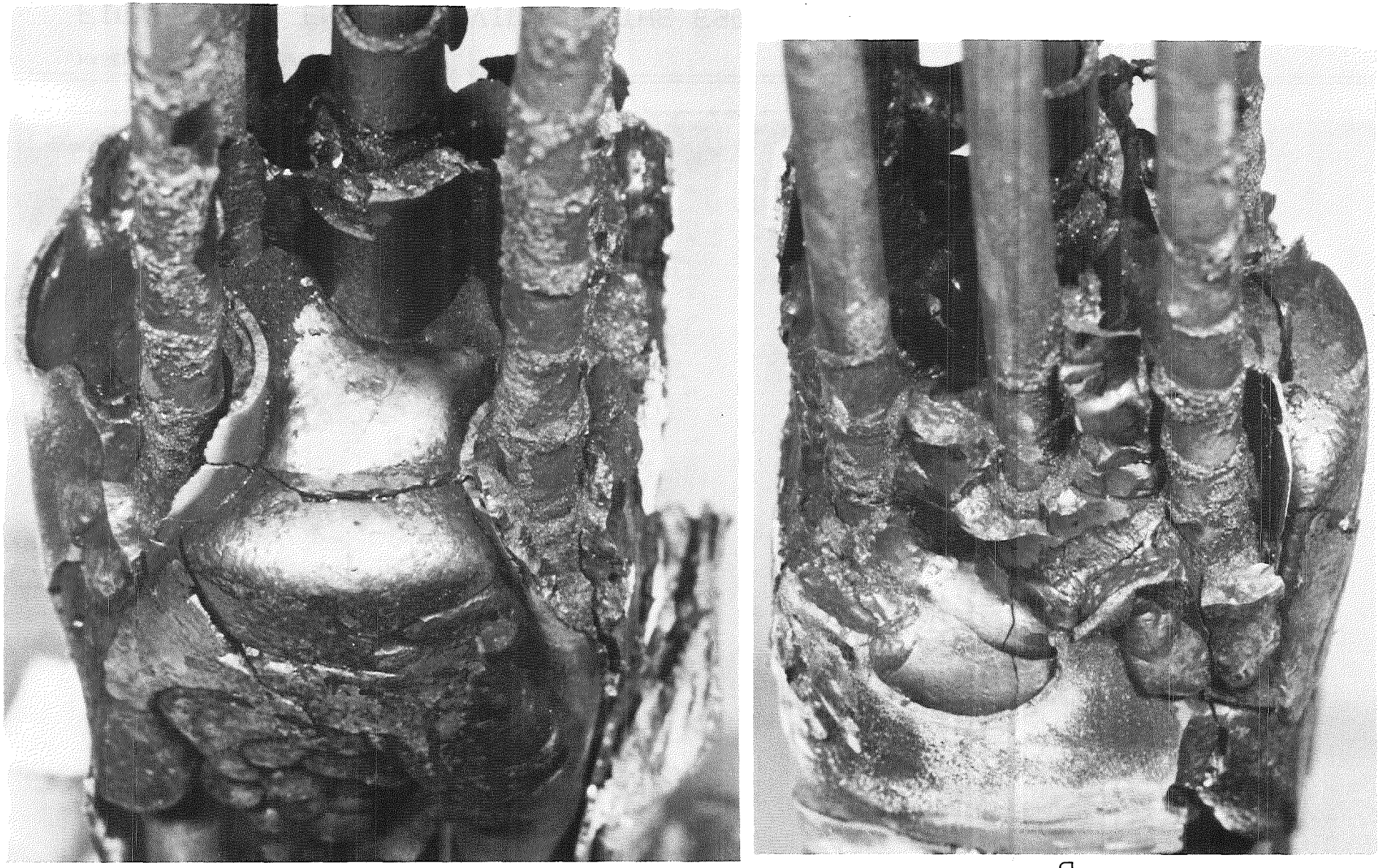

FIGURE 19: ENLARGED VIEW OF THE ESBU-2A BLOCKED REGION FROM ABOVE: TWO ORIENTATIONS

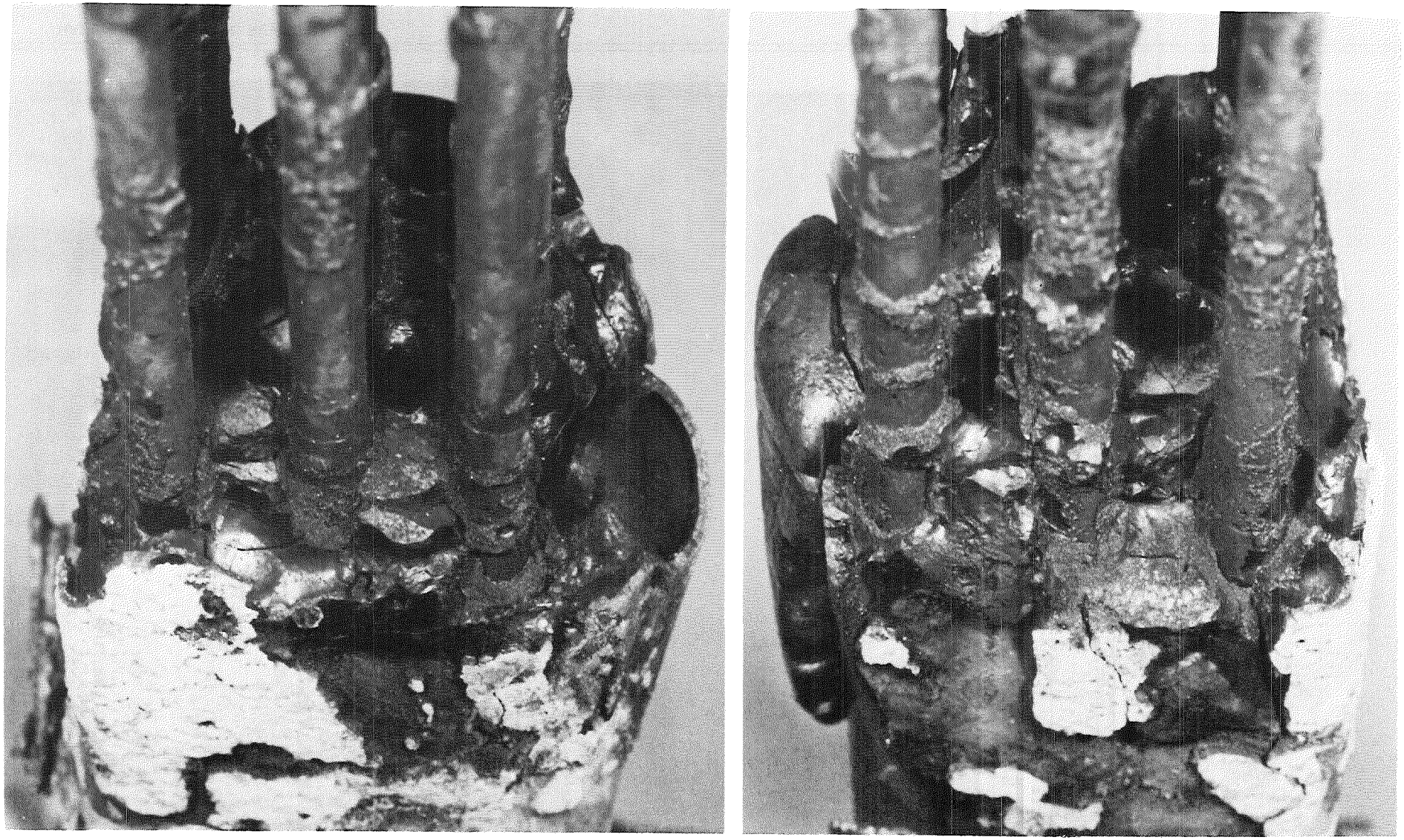

FIGURE 20: ENLARGED VIEW OF THE ESBU-2A BLOCKED REGION FROM ABOVE: TWO ORIENTATIONS

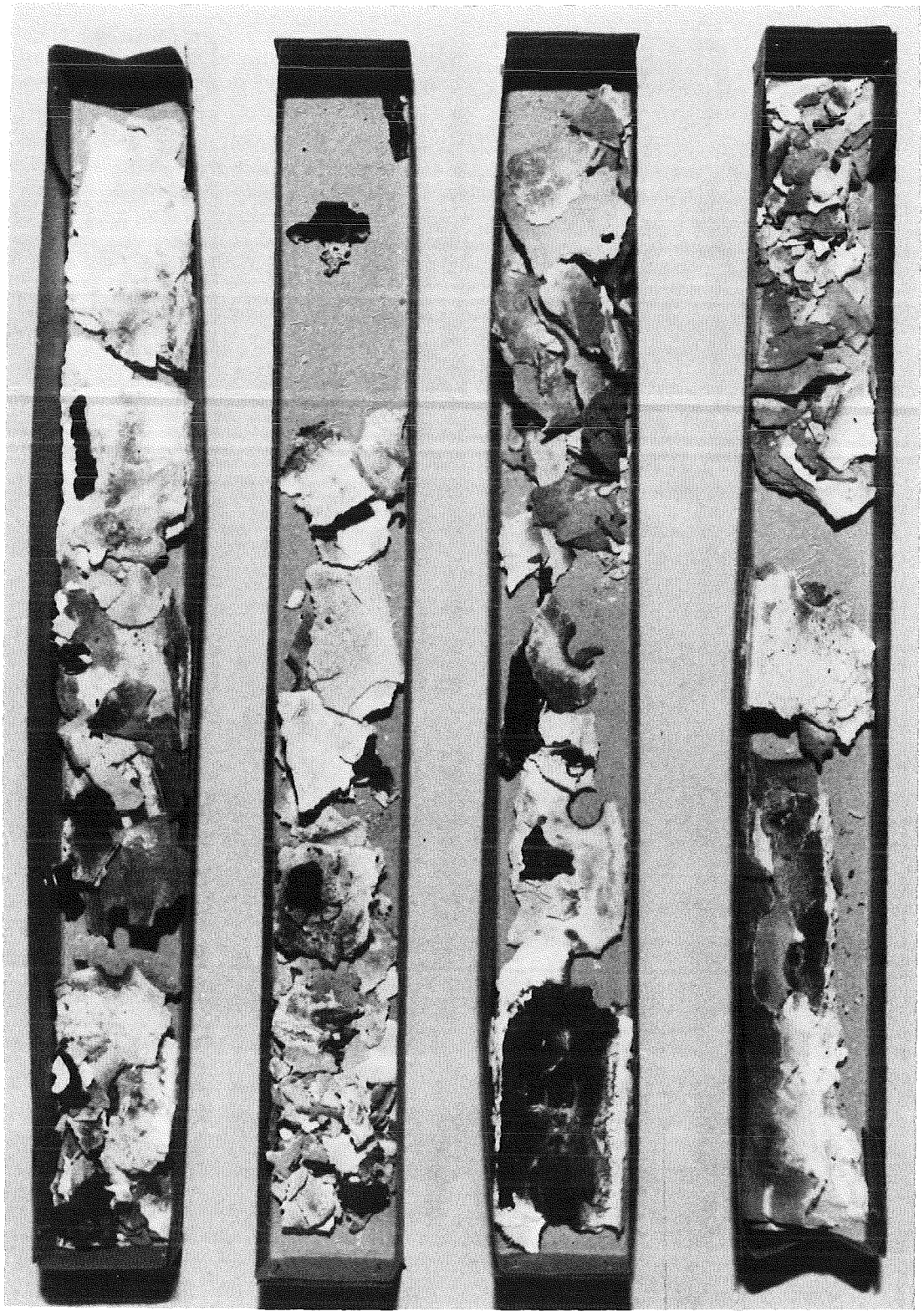

FIGURE 21: POSTTEST APPEARANCE OF THE ESBU-2A INSULATION AFTER REMOVAL

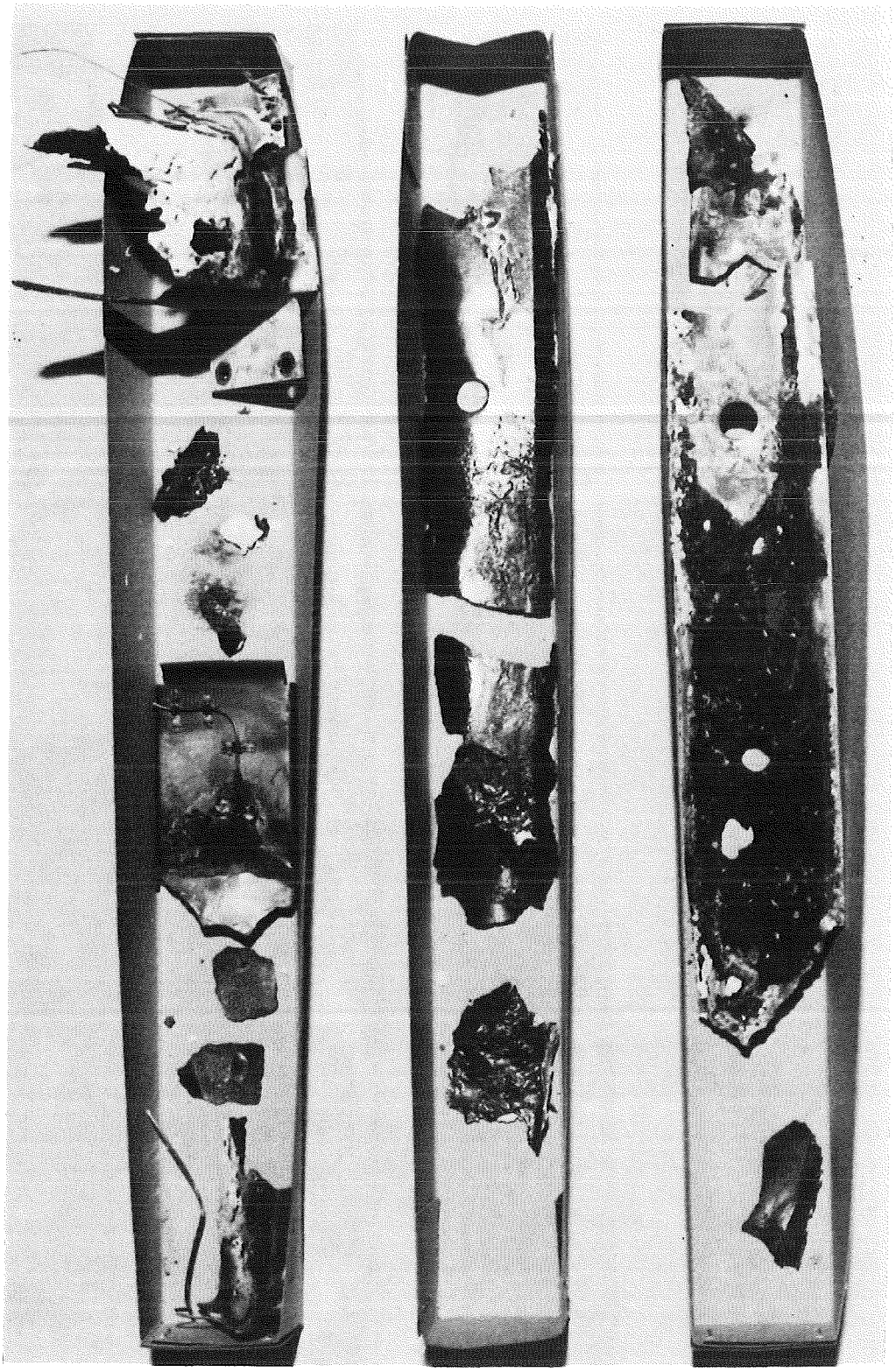

FIGURE 22: POSTTEST APPEARANCE OF THE ESBU-2A SHROUD AFTER REMOVAL

FIGURE 23: CLOSE-UP OF THE ESBU-2A SHROUD SHOWING THE OUTER SURFACES

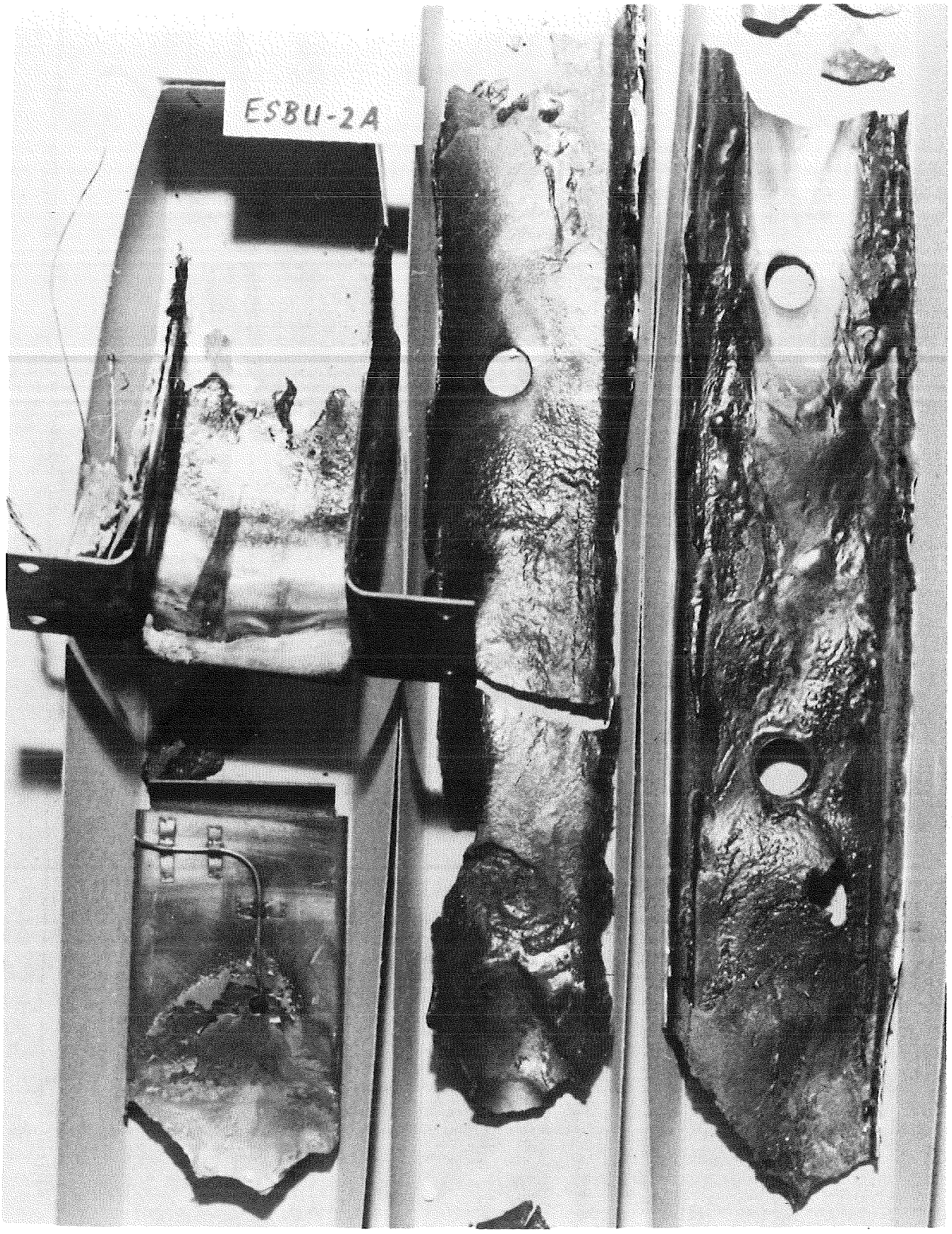

FIGURE 24: CLOSE-UP OF THE ESBU-2A SHROUD SHOWING THE INNER SURFACES

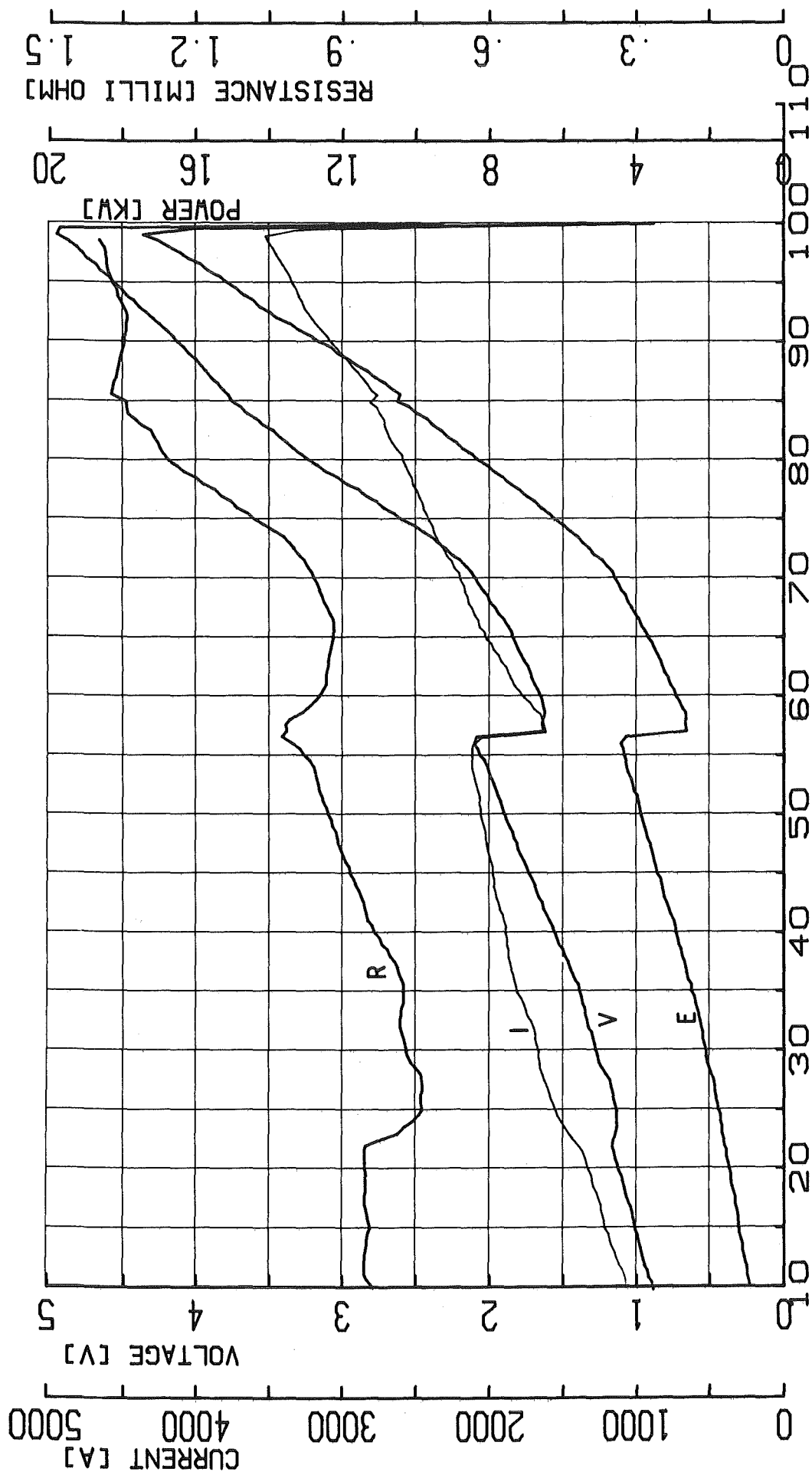

FIG.25: VOLTAGE V, CURRENT I, ELECTRIC POWER E AND RESISTANCE R FOR TEST ESBU-2A

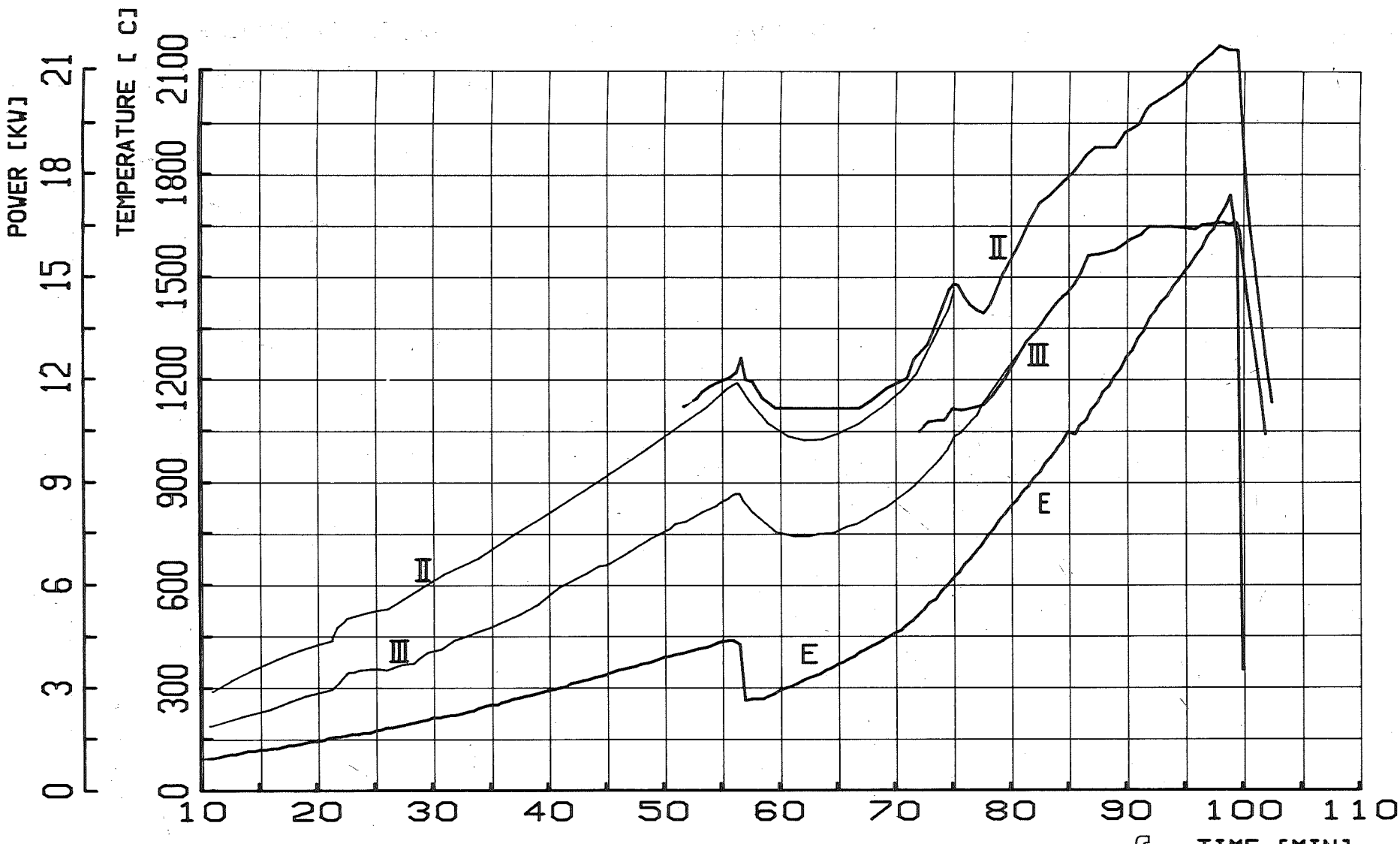

HAGEN ET AL. KFK-REPORT 3509

PNS KfK IT

FIG. 26: TEMPERATURES ON THE CENTRAL ROD (5) AT THE 255 (II) AND 345 MM (III) ELEVATIONS COMPARED TO THE ELECTRIC POWER (E). : ESBU-2A

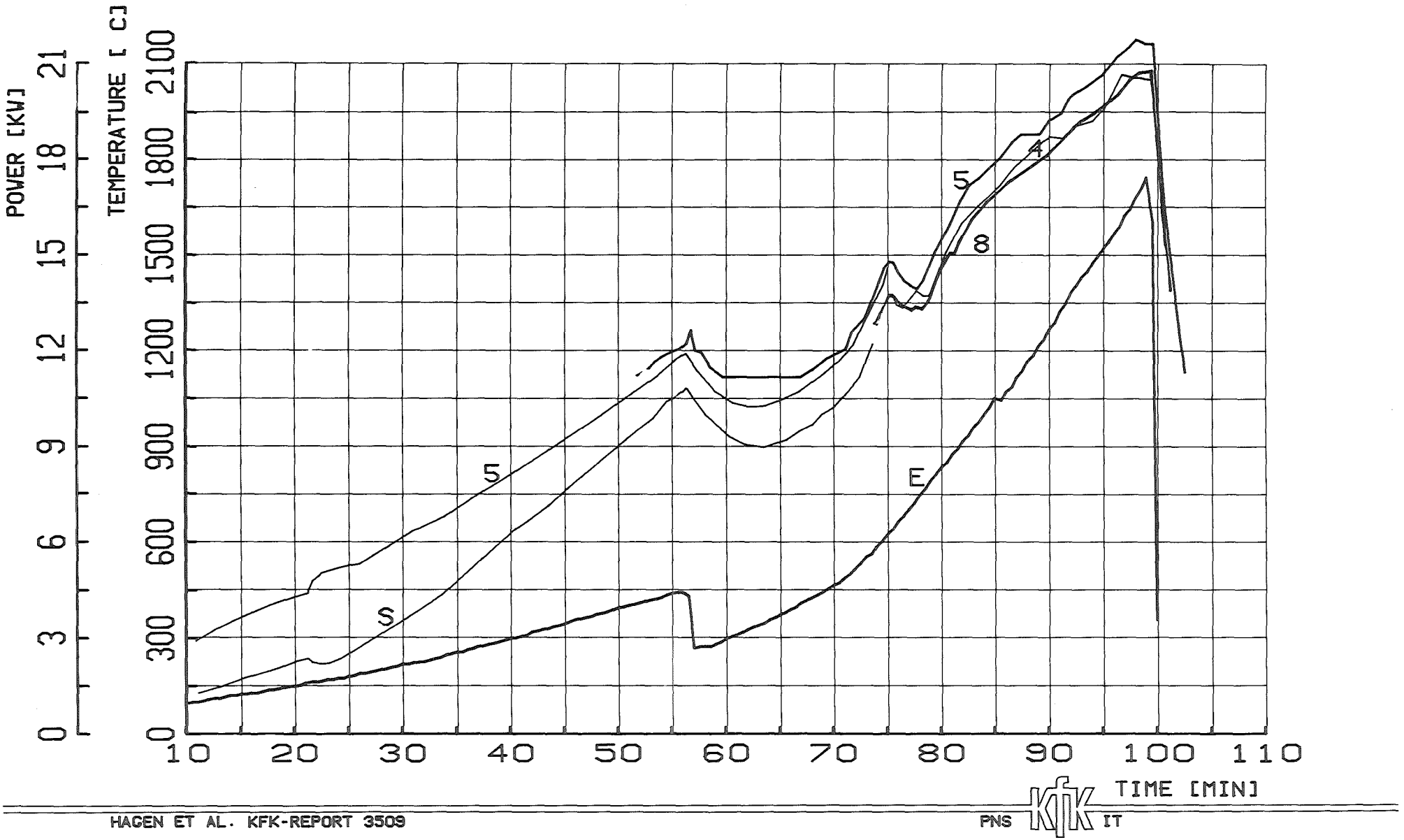

HAGEN ET AL. KFK-REPORT 3509 PNS KfK IT

FIG. 27: TEMPERATURES AT THE 255 MM MIDPLANE ON THE CENTRAL ROD (5), SIDE RODS (4+8) AND SHROUD (S) COMPARED TO THE ELECTRIC POWER (E). : ESBU-2A

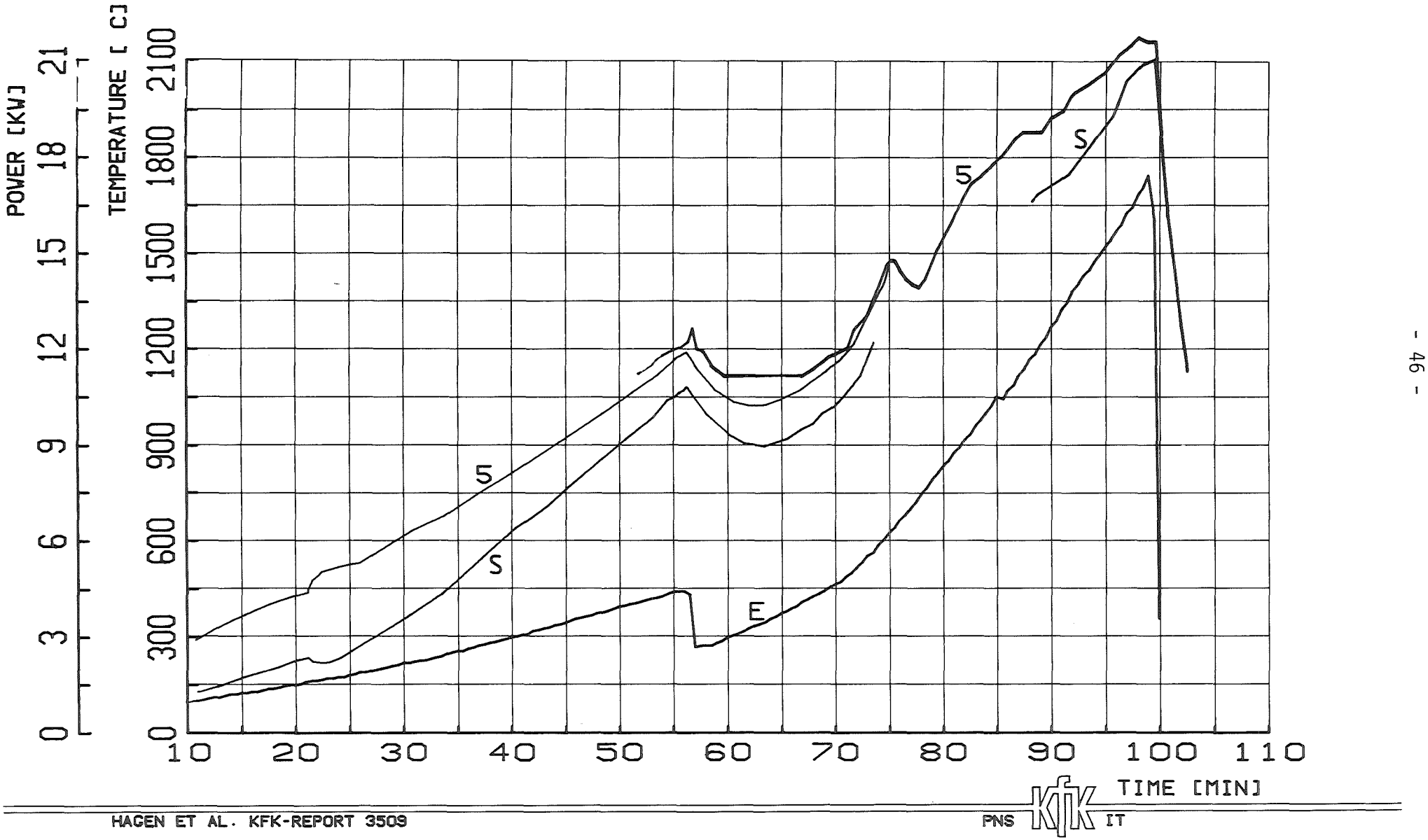

FIG. 28: TEMPERATURES AT THE 255 MM MIDPLANE ON THE CENTRAL ROD (5) AND THE SHROUD (S) IN COMPARISON TO THE ELECTRIC POWER (E). : ESBU-2A

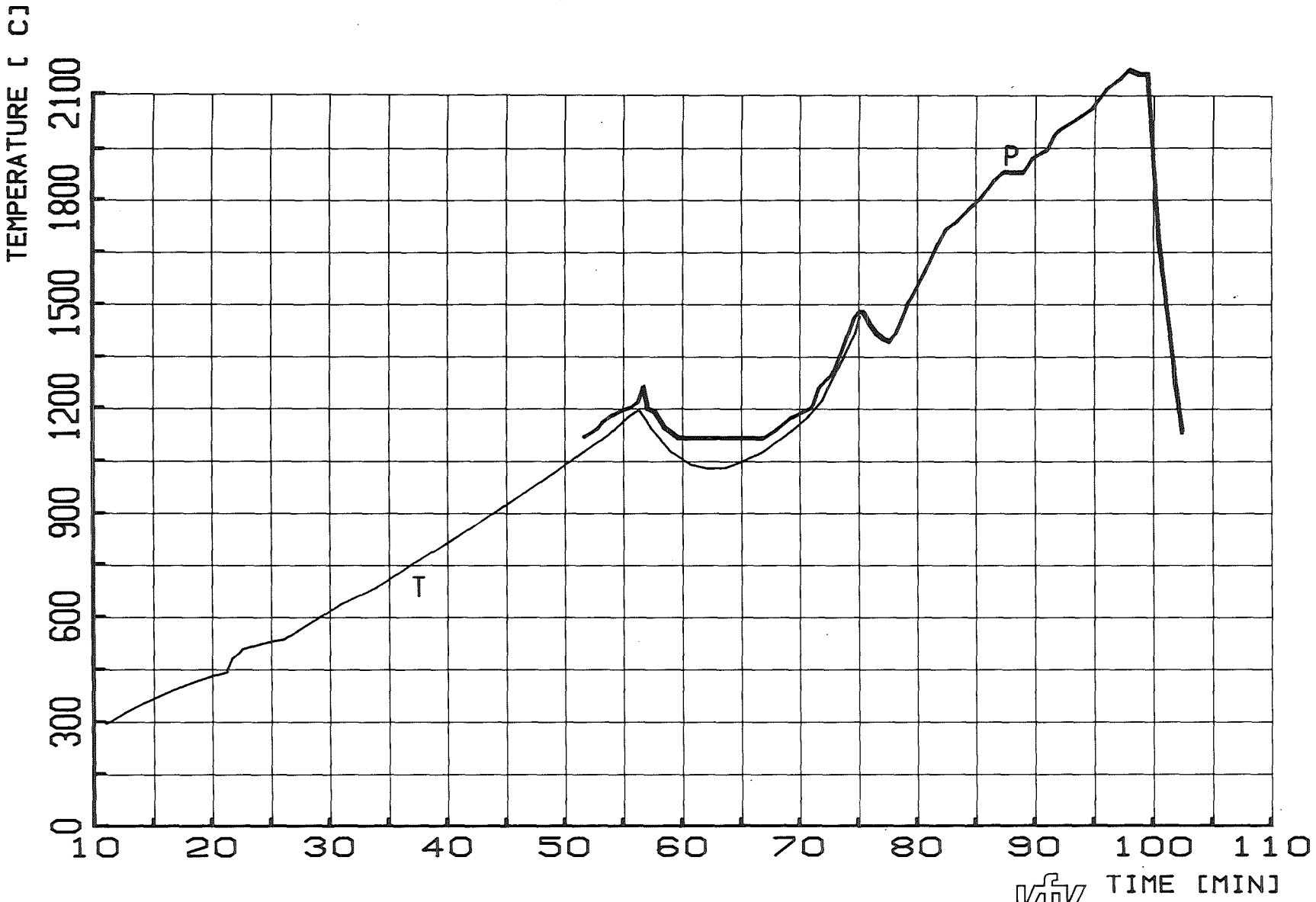

FIG. 29: TEMPERATURES MEASURED BY THERMOCOUPLE AND TWO COLOR PYROMETER ON CENTRAL ROD (5) AT 255 MM ELEVATION (II). : ESBU-2A

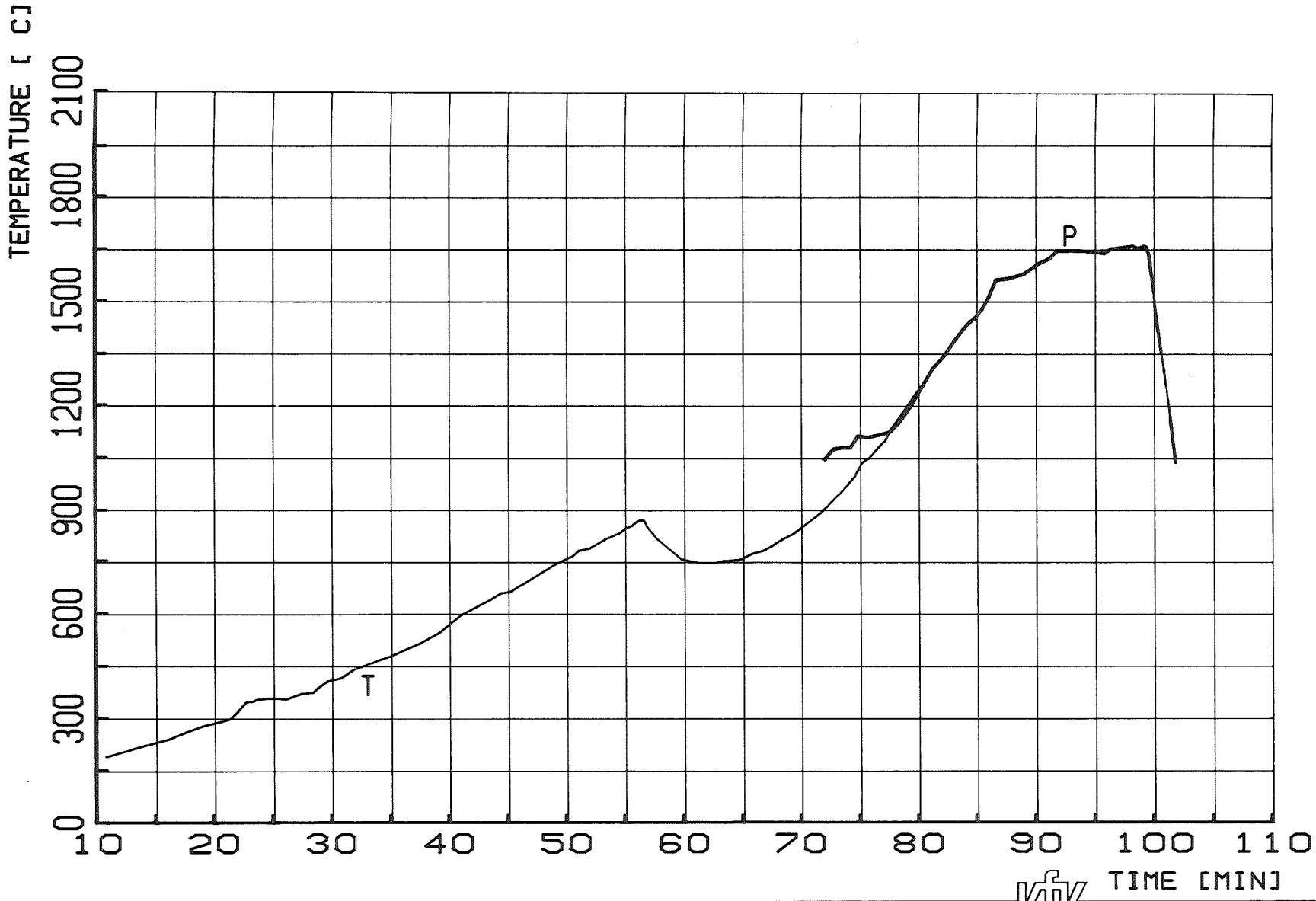

FIG. 30: TEMPERATURES MEASURED BY THERMOCOUPLE AND TWO COLOR PYROMETER ON CENTRAL ROD (5) AT 345 MM ELEVATION (III). : ESBU-2A

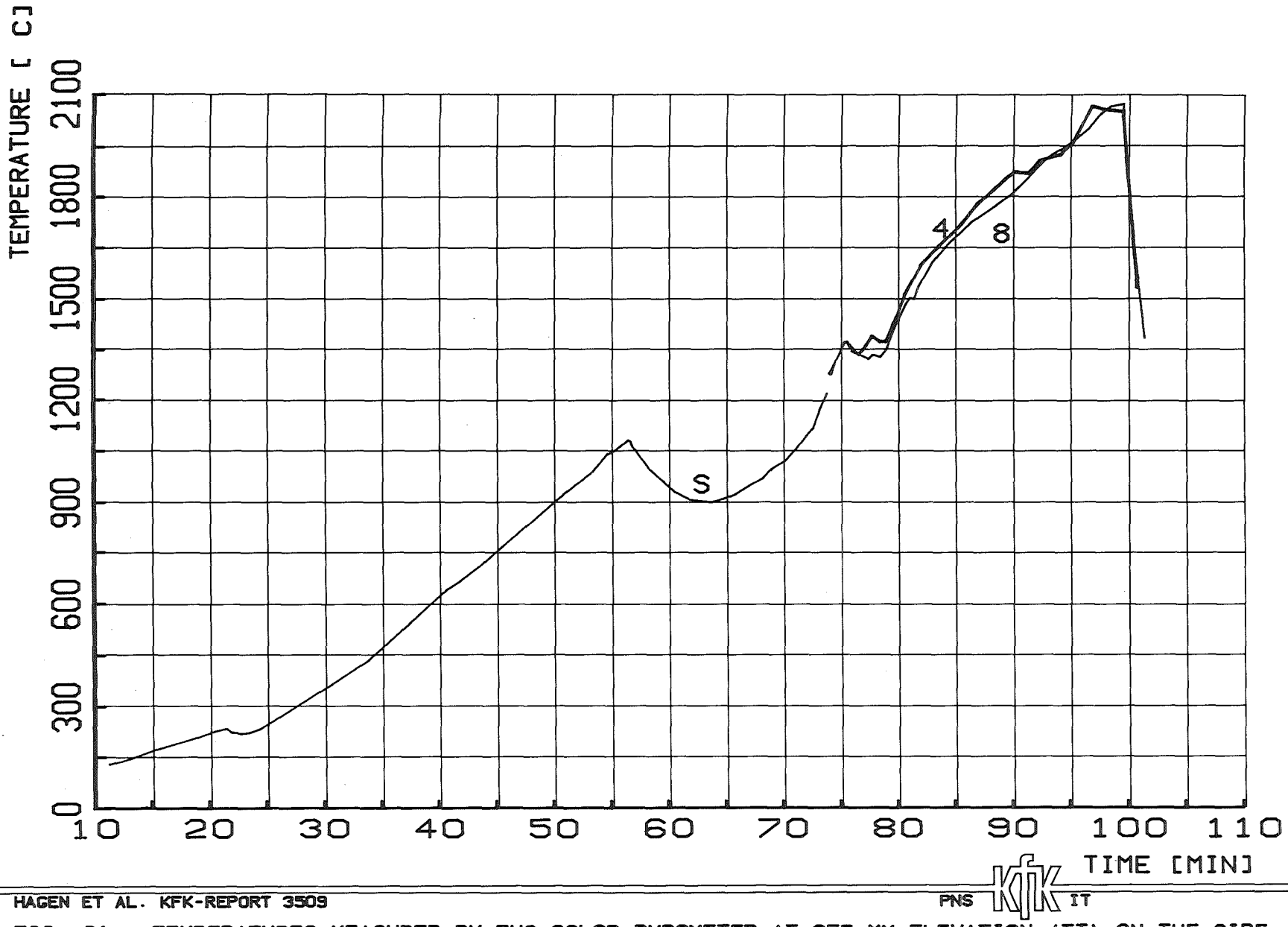

FIG. 31: TEMPERATURES MEASURED BY TWO COLOR PYROMETER AT 255 MM ELEVATION (II) ON THE SIDE RODS (4+8). COMPARED TO THERMOCOUPLE MEASUREMENTS ON THE SHROUD (S). : ESBU-2A

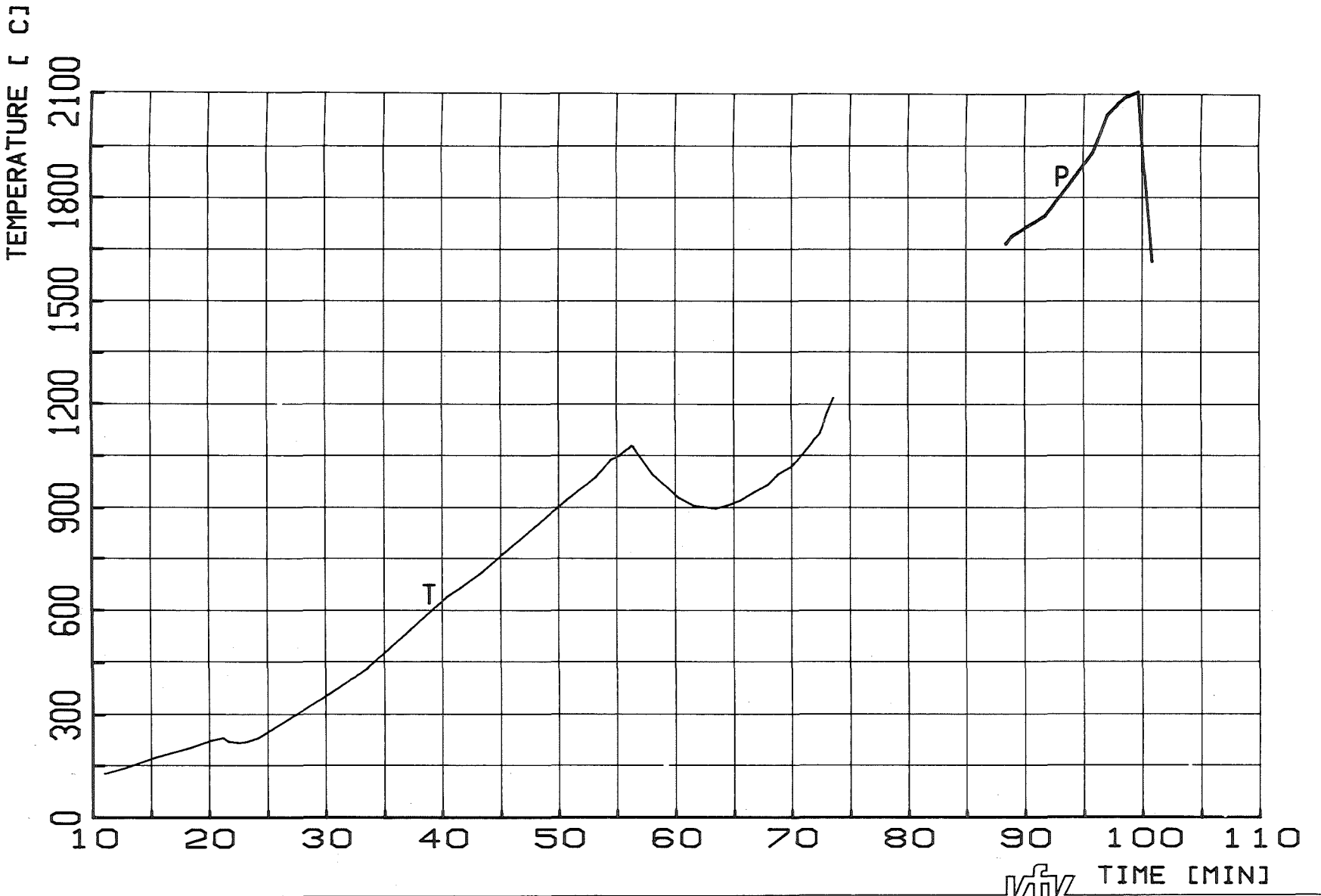

FIG. 32: TEMPERATURES MEASURED BY THERMOCOUPLE AND TWO COLOR PYROMETER ON THE SHROUD AT THE 255 MM ELEVATION (II). : ESBU-2A

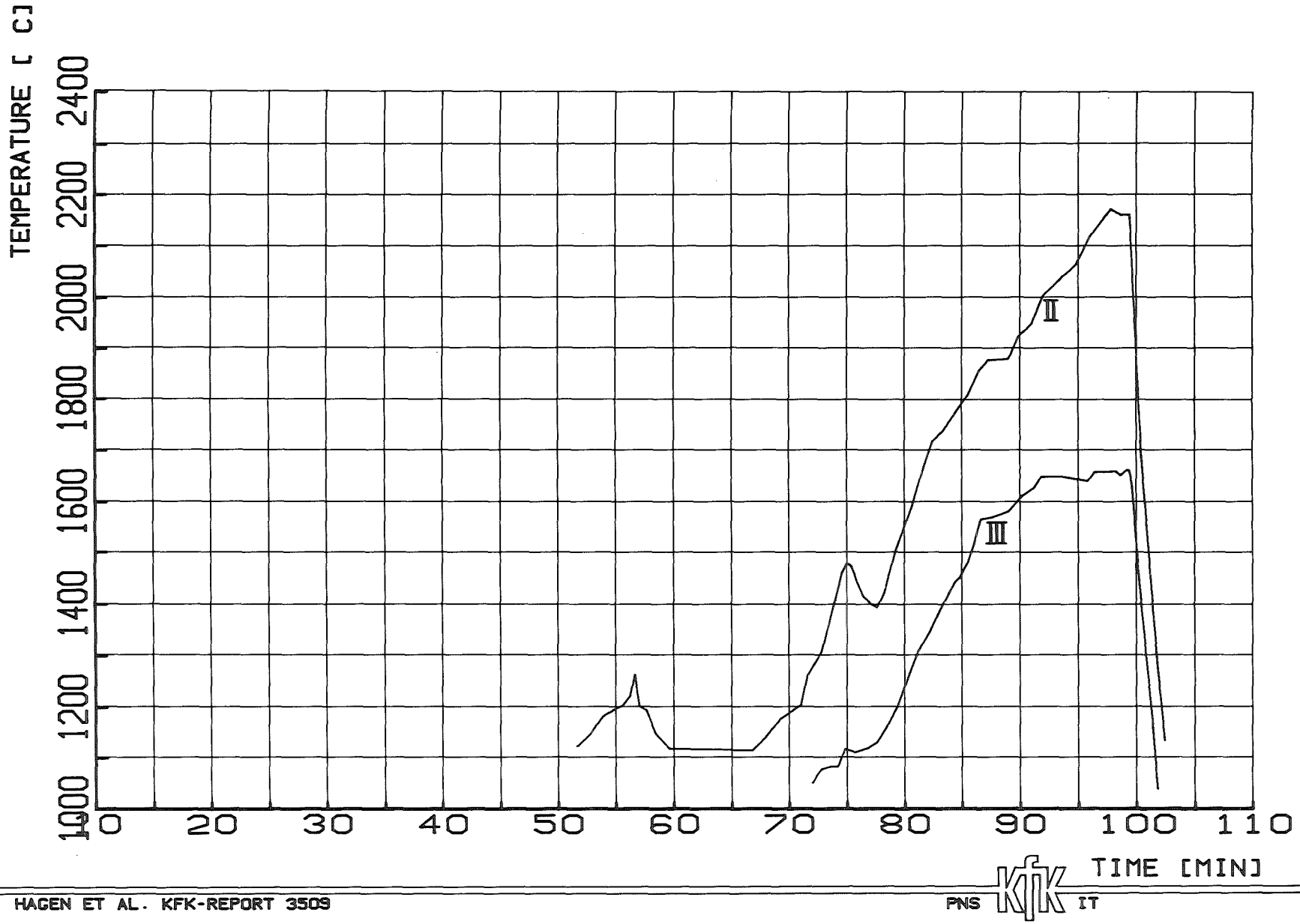

FIG. 33: TEMPERATURES MEASURED BY TWO COLOR PYROMETERS ON THE CENTRAL ROD (5), AT THE 255 MM (II) AND THE 345 MM ELEVATION (III). : ESBU-2A

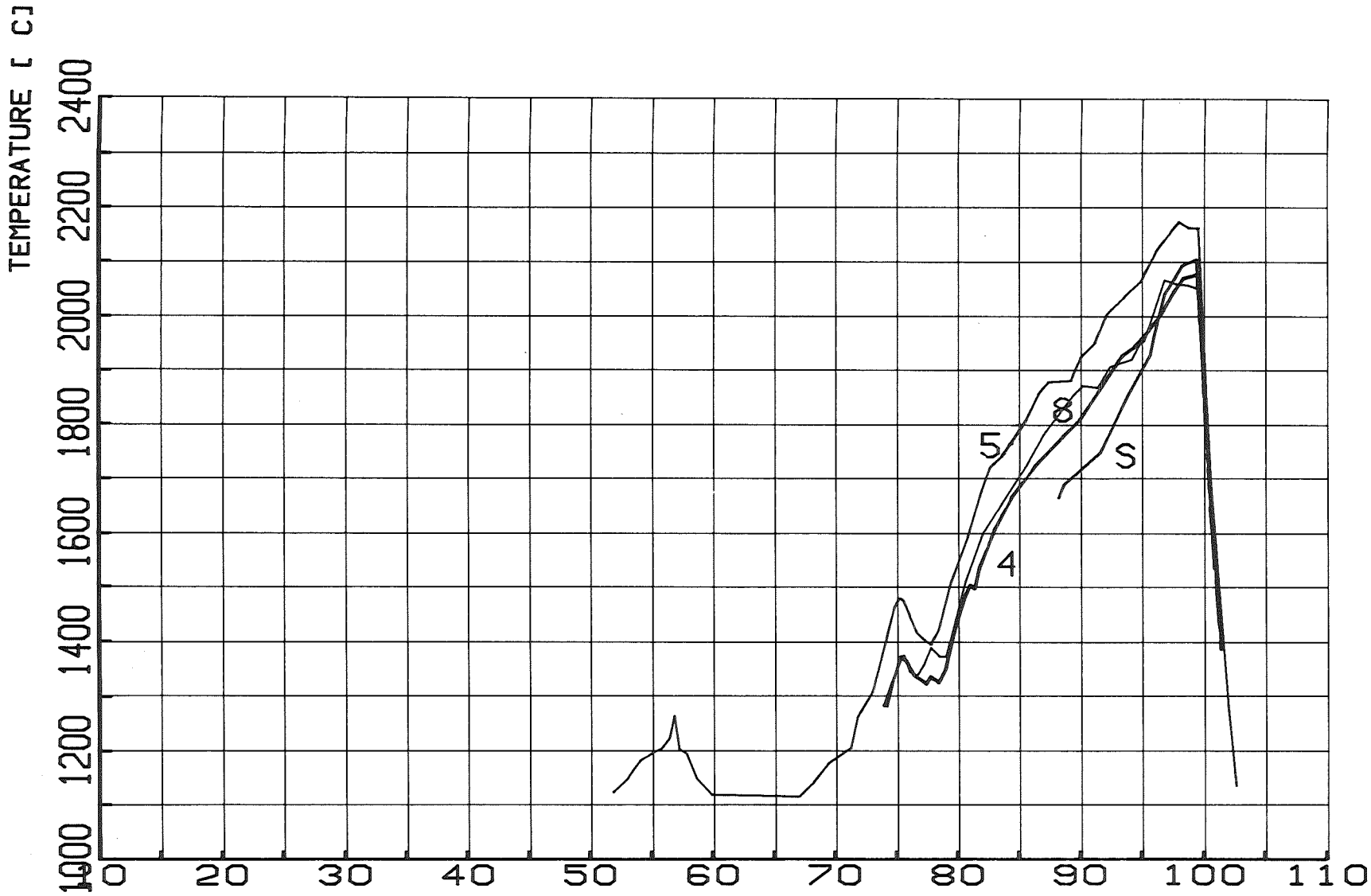

FIG. 34: TEMPERATURES MEASURED BY TWO COLOR PYROMETERS AT THE 255 MM MIDPLANE (II) ON THE CENTRAL ROD (5), TWO SIDE RODS (4+8) AND THE SHROUD (S). : ESBU-2A

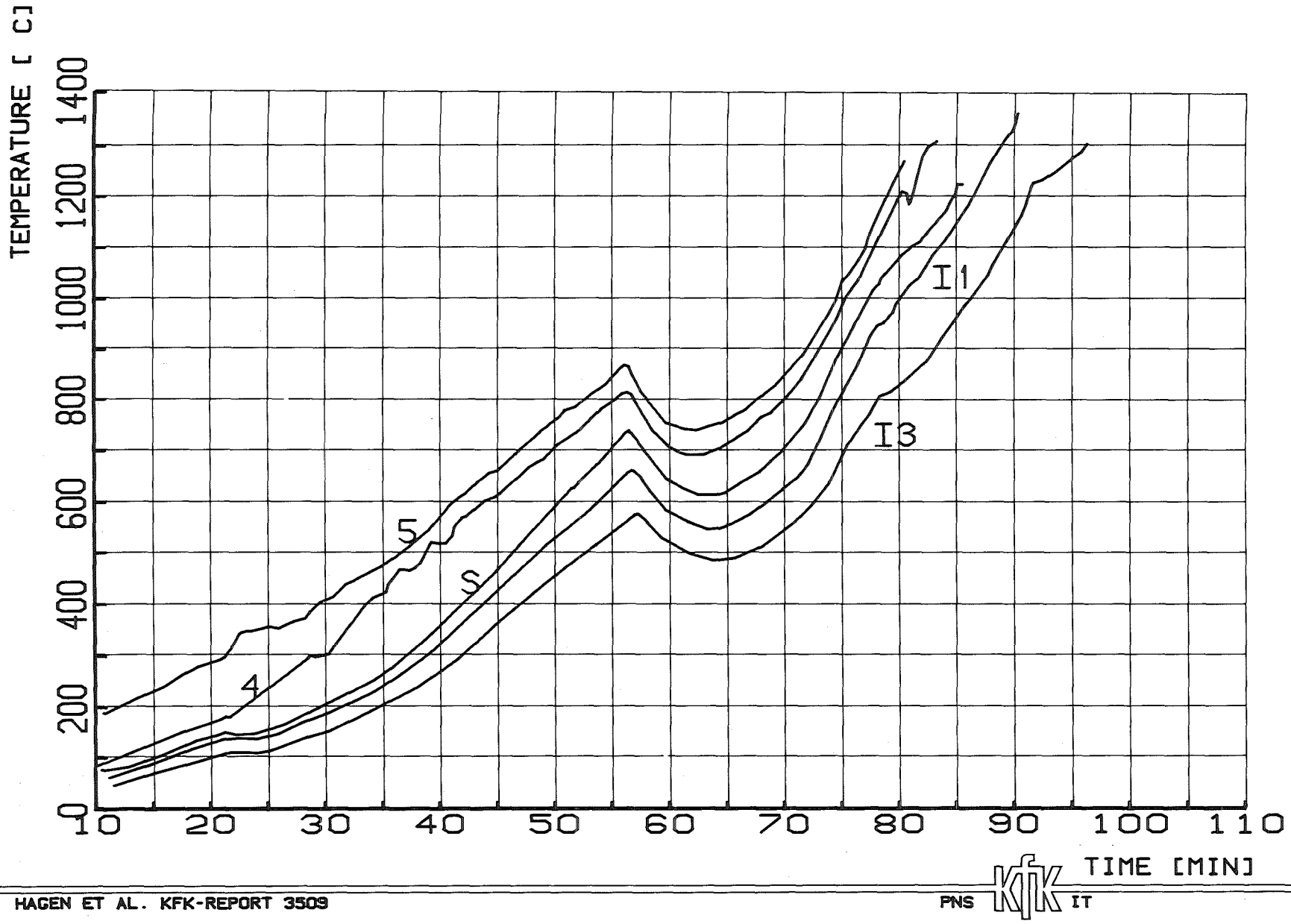

FIG. 35: TEMPERATURES AT THE 345 MM ELEVATION ON CENTRAL ROD (5), SIDE ROD (4), SHROUD (S) AND 1.3 MM (I1) AND 3.8 MM (I3) INTO THE FIBER CERAMIC INSULATION. :ESBU-2A

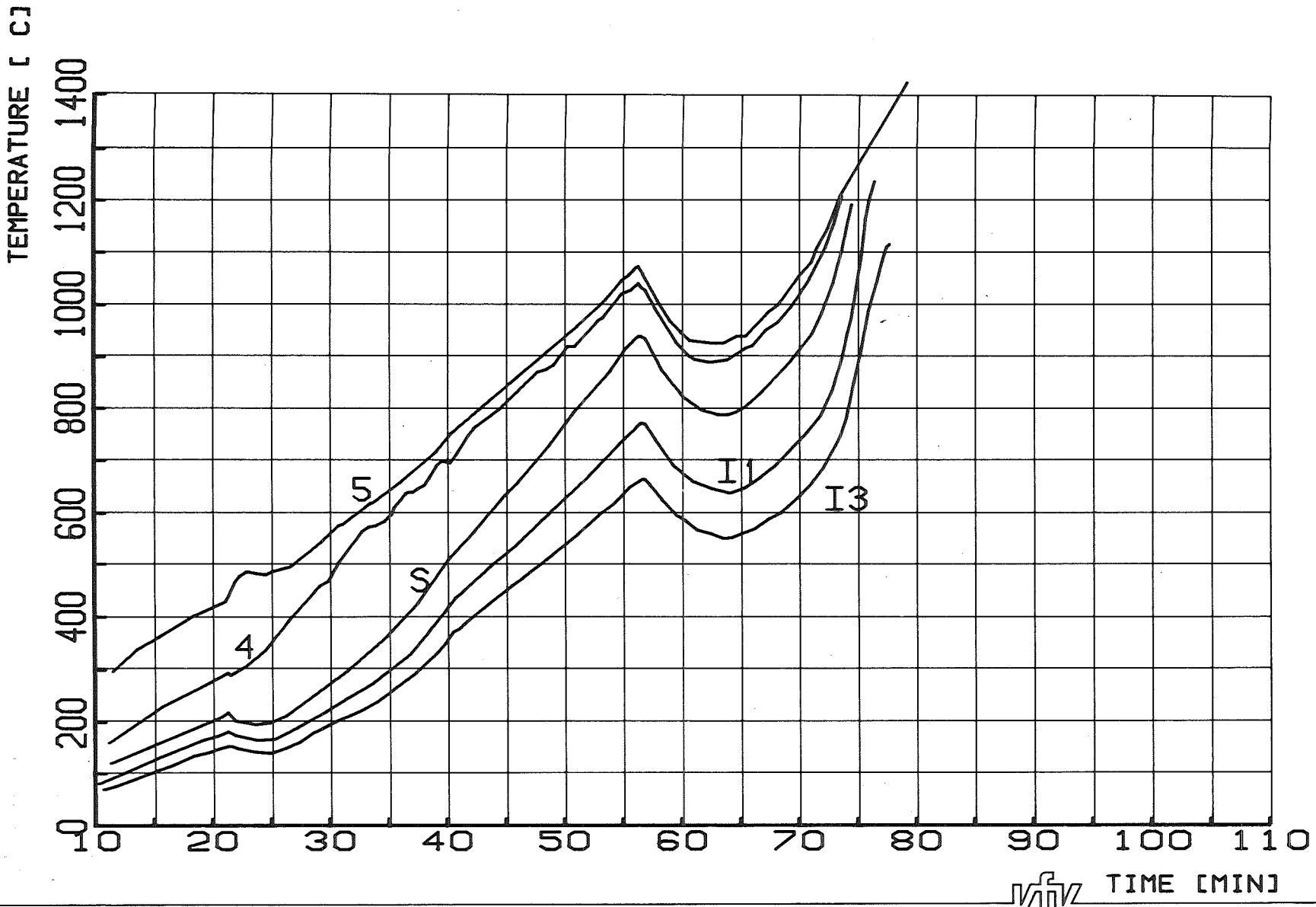

FIG. 36: TEMPERATURES AT THE 155 MM ELEVATION ON CENTRAL ROD (5), SIDE ROD (4), SHROUD (S) AND 1.3 MM (I1) AND 3.8 MM (I3) INTO THE FIBER CERAMIC INSULATION. :ESBU-2A

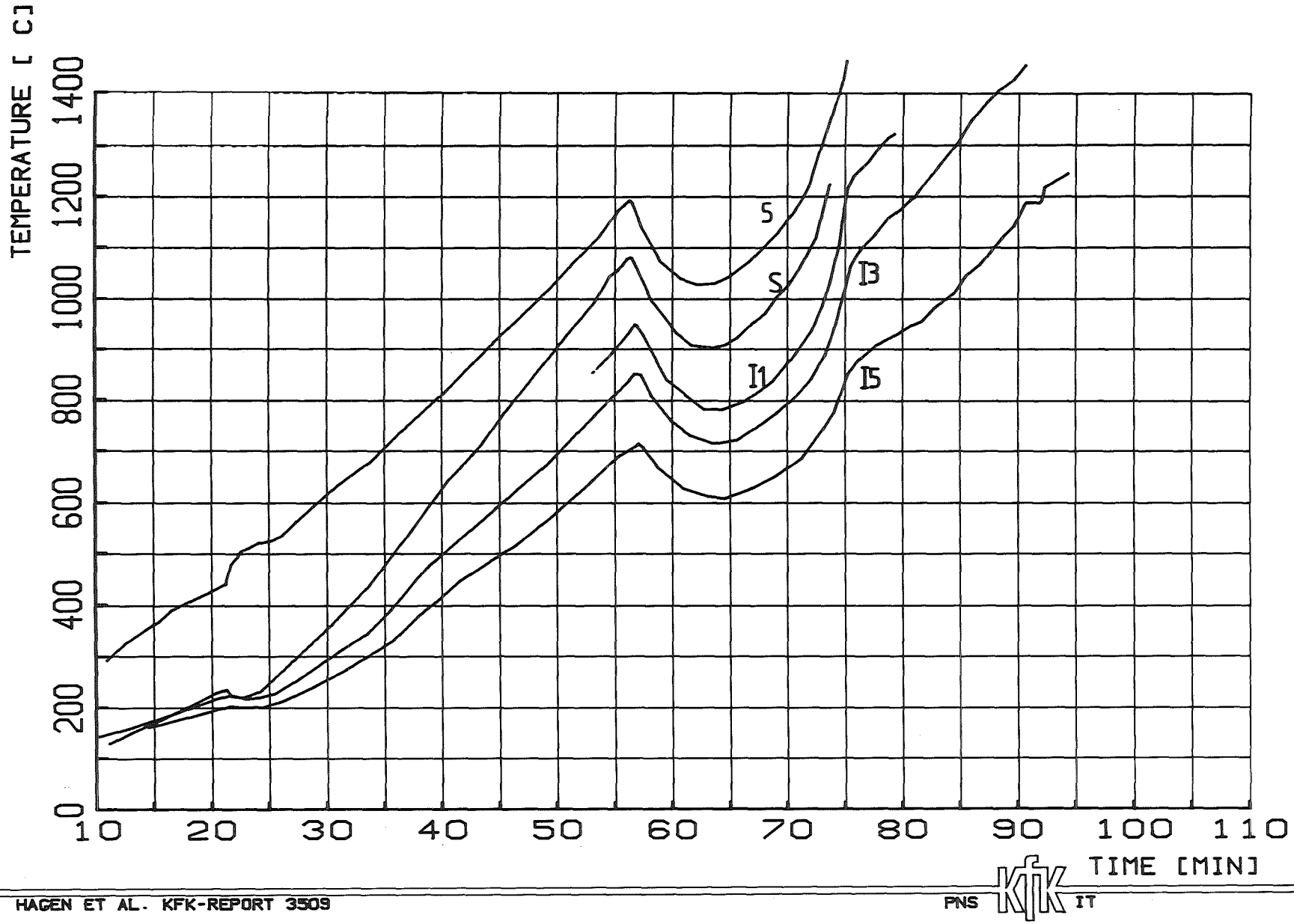

FIG. 37: TEMPERATURES AT THE 255 MM (II) ELEVATION ON CENTRAL ROD (5), SHROUD (S) AND 1.3 MM (I1), 3.8 MM (I3) AND 6.4 MM (I5) INTO THE FIBER CERAMIC INSULATION. :ESBU-2A

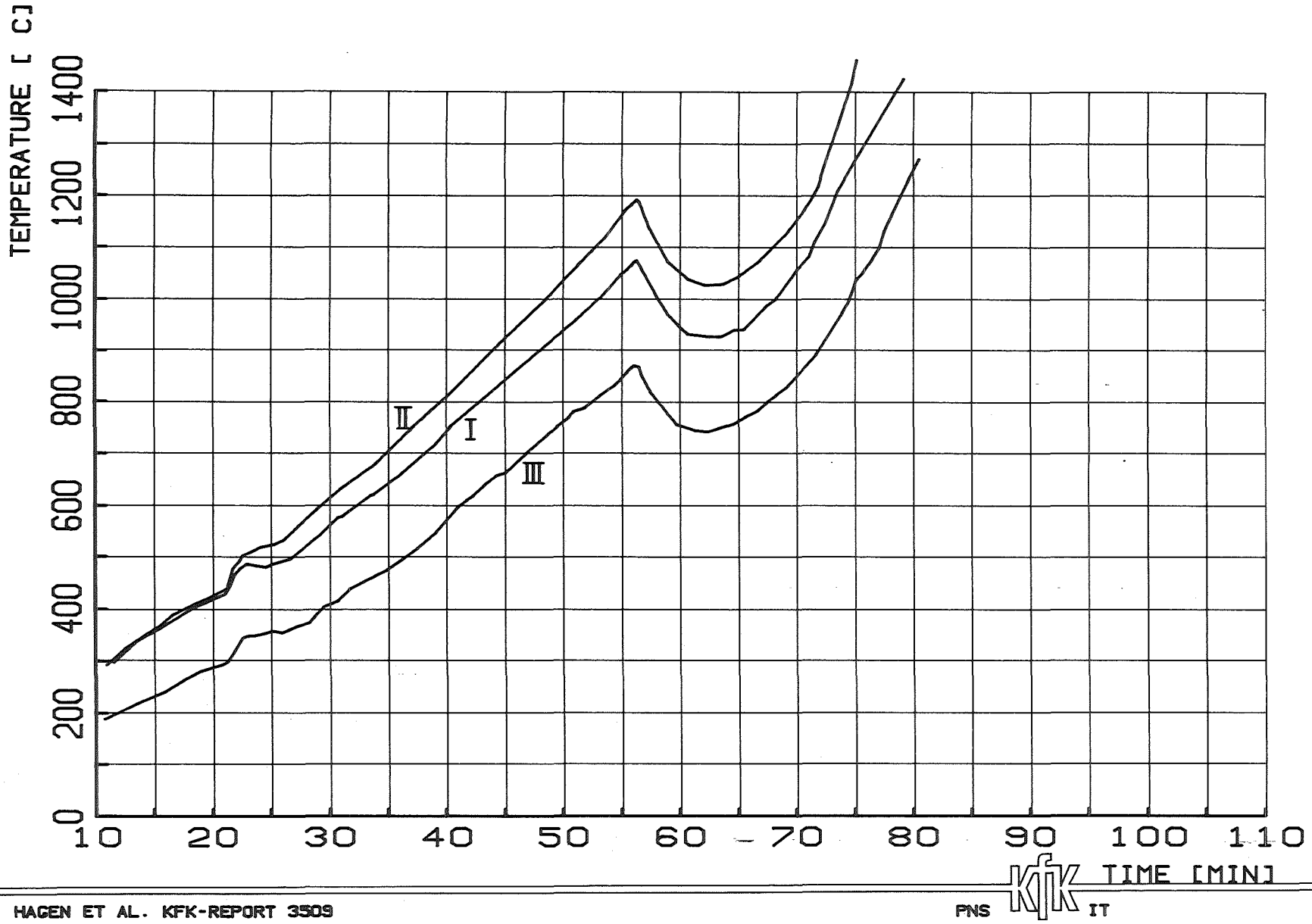

FIG. 38: TEMPERATURES ON THE CENTRAL ROD (5) AT 155 MM (I), 255 MM (II) AND 345 MM (III) ELEVATIONS. : ESBU-2A

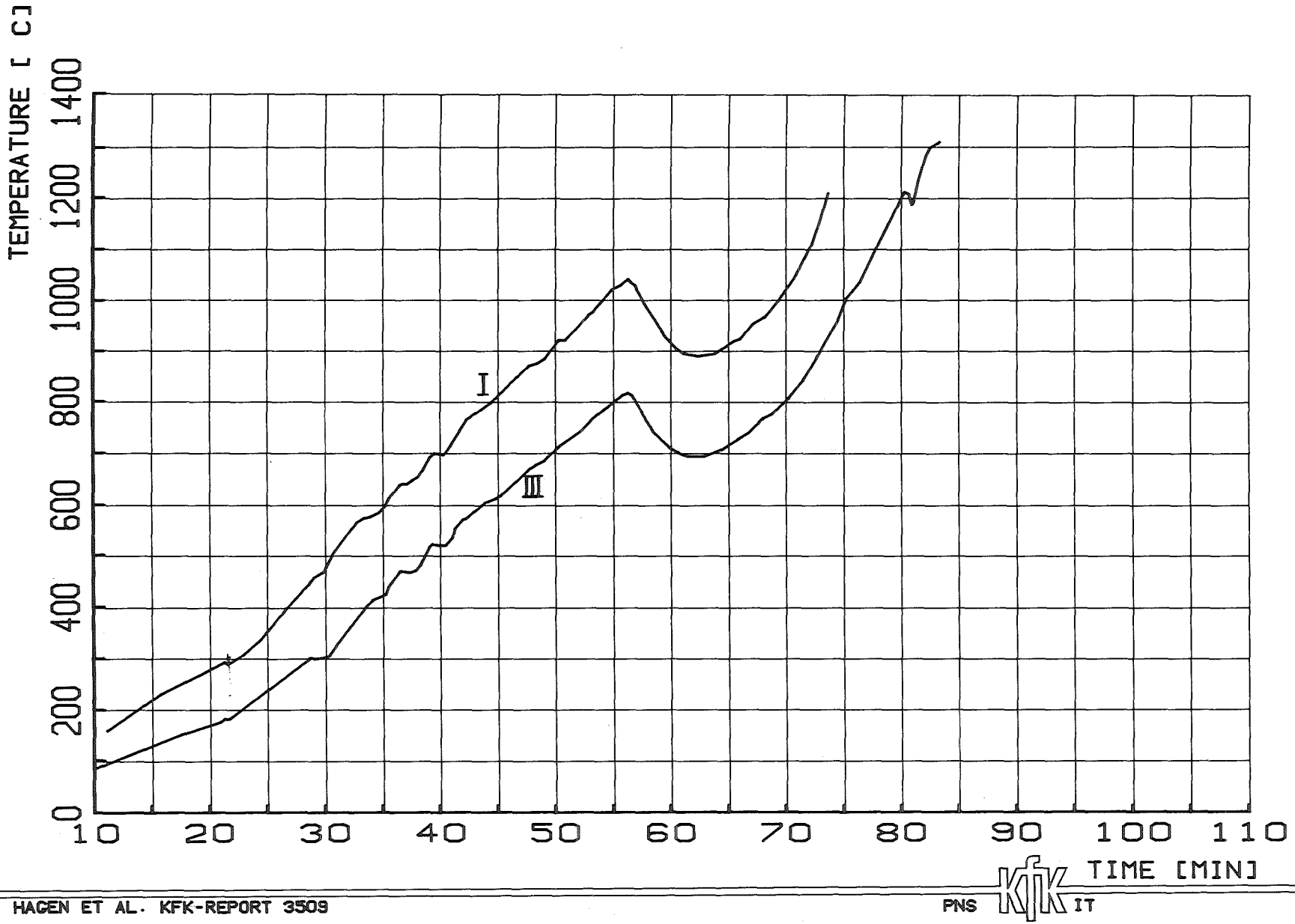

FIG. 39: TEMPERATURES ON THE SIDE ROD (4) AT THE 155 MM (I) AND 345 MM (III) ELEVATIONS. : ESBU-2A

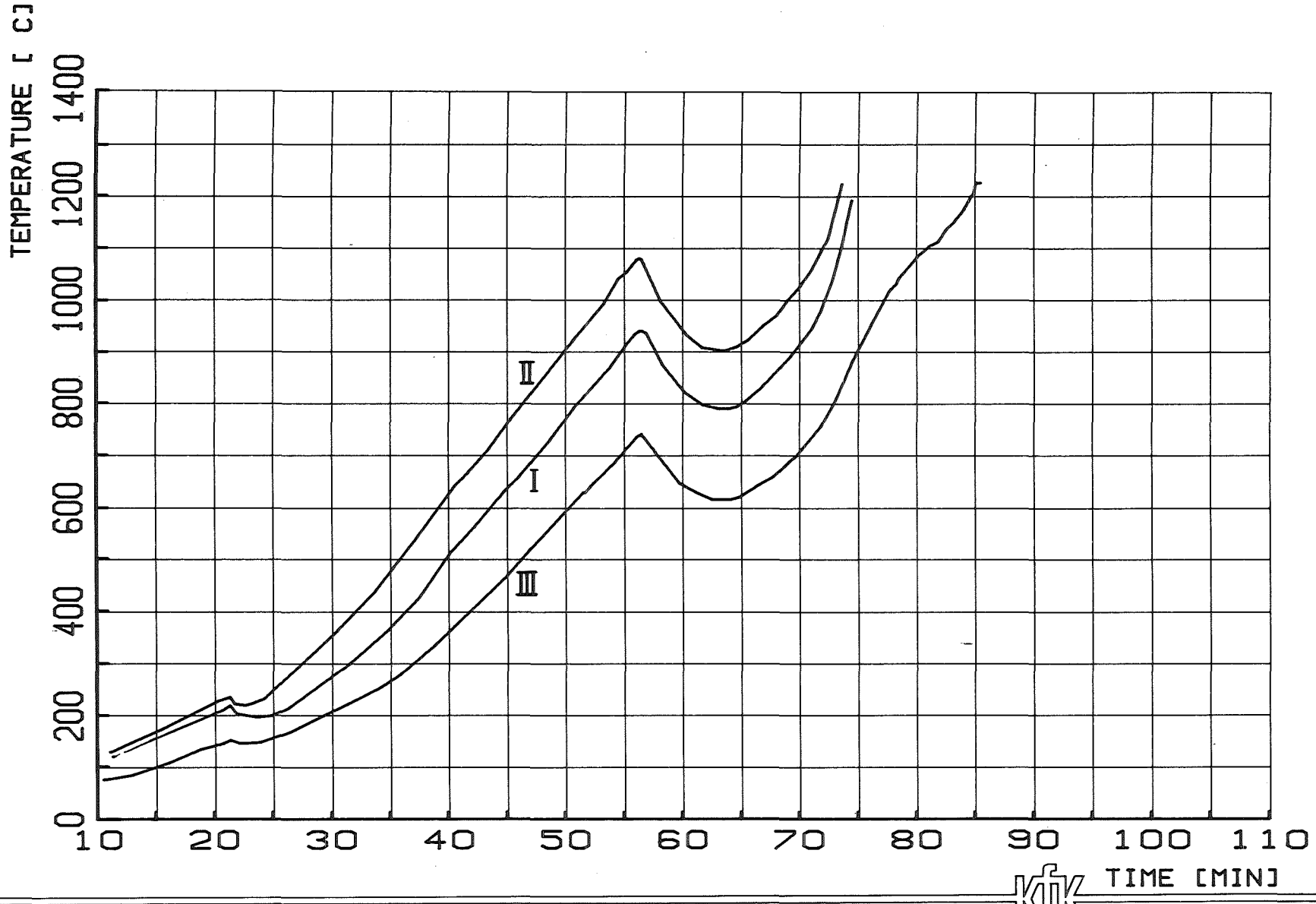

FIG. 40: TEMPERATURES ON THE SHROUD (S) AT THE 155 MM (I), 255 MM (II) AND 345 MM (III) ELEVATIONS. :ESBU-2A

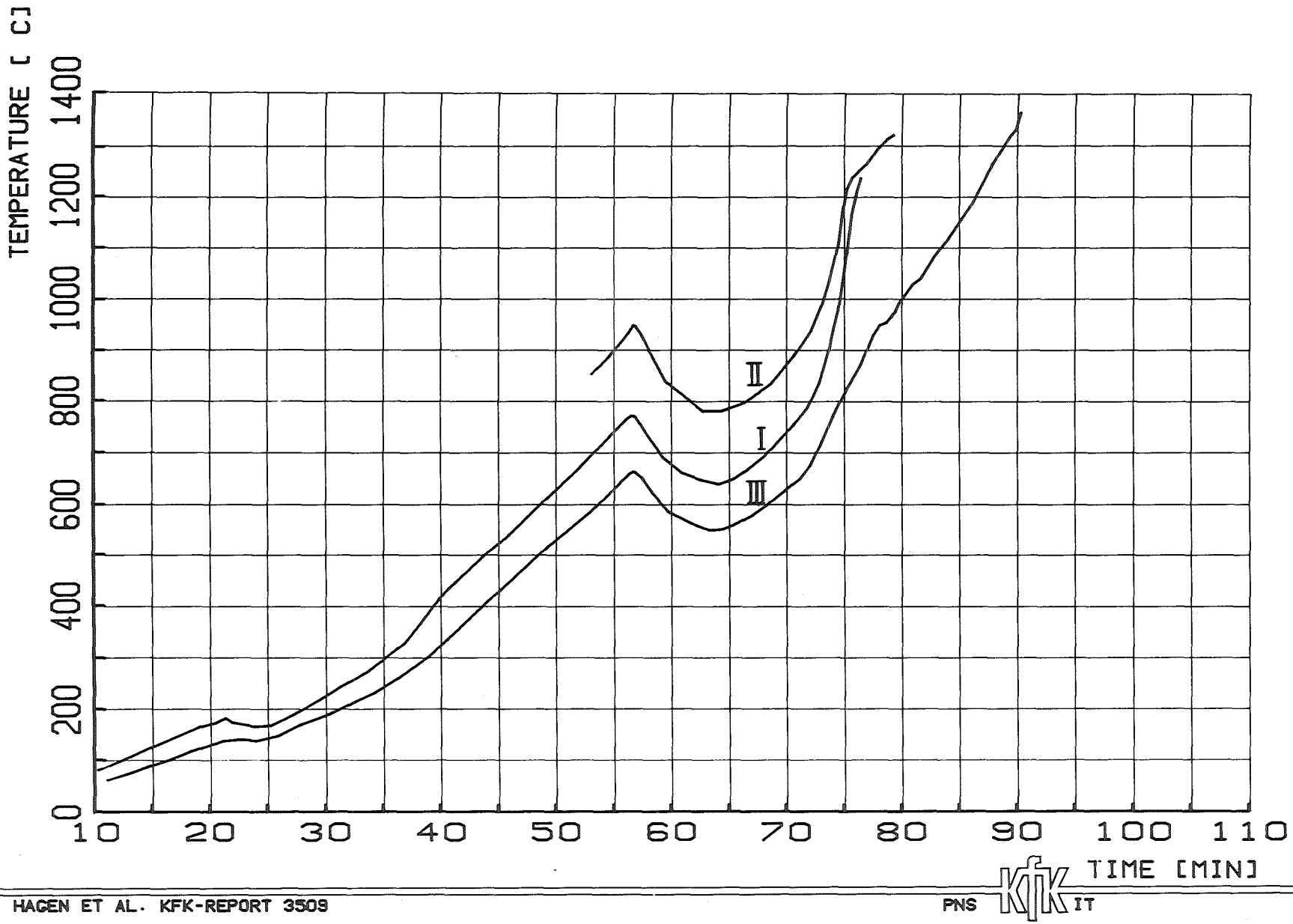

FIG. 41: TEMPERATURES IN THE INSULATION 1.3 MM INTO THE FIBER CERAMIC AT THE 155 MM (I), 255 MM (II) AND 345 MM (III) ELEVATIONS. : ESBU-2A

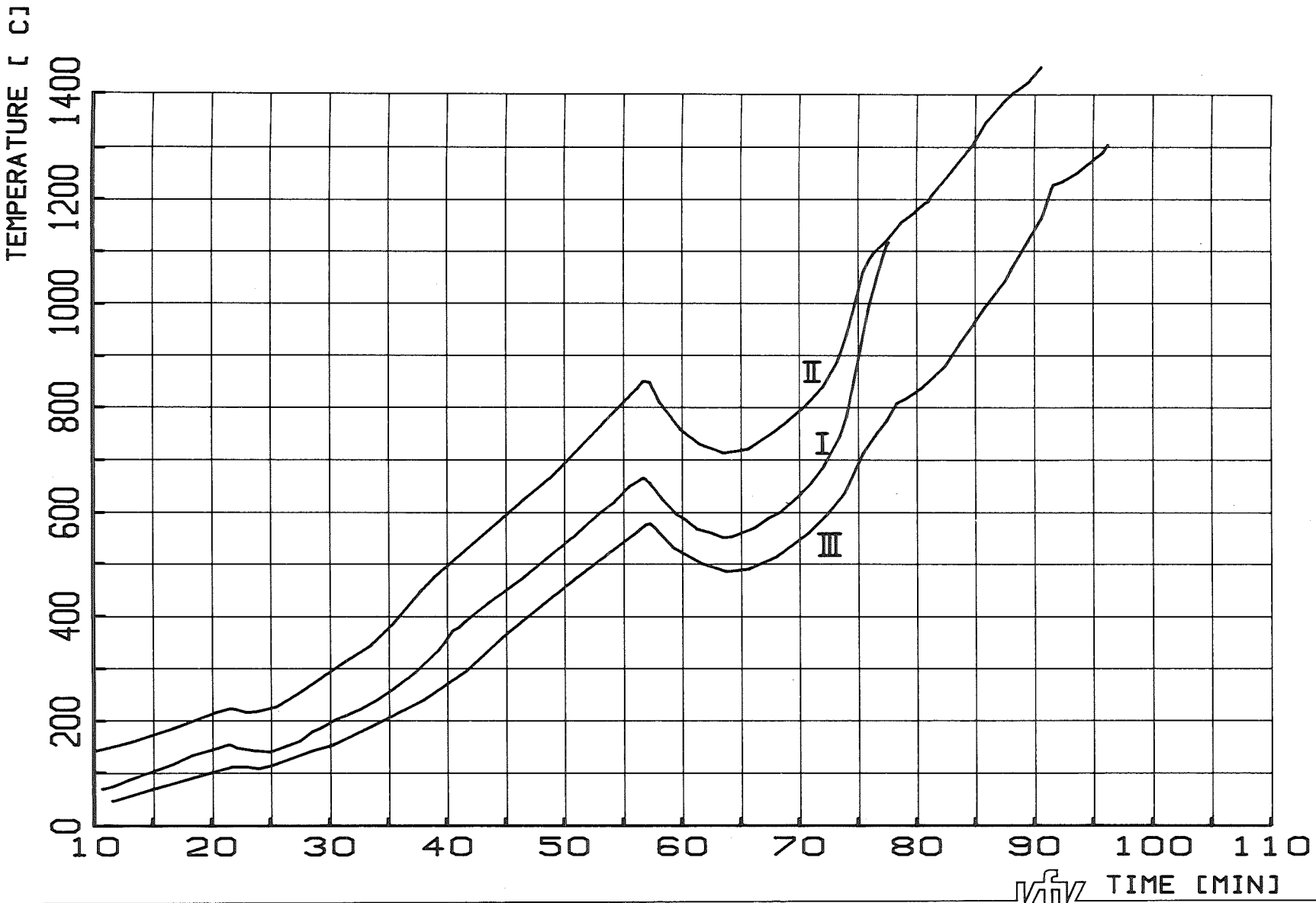

FIG. 42: TEMPERATURES IN THE INSULATION 3.8 MM INTO THE FIBER CERAMIC AT THE 155 MM (I), 255 MM (II) AND 345 MM (III) ELEVATIONS. : ESBU-2A

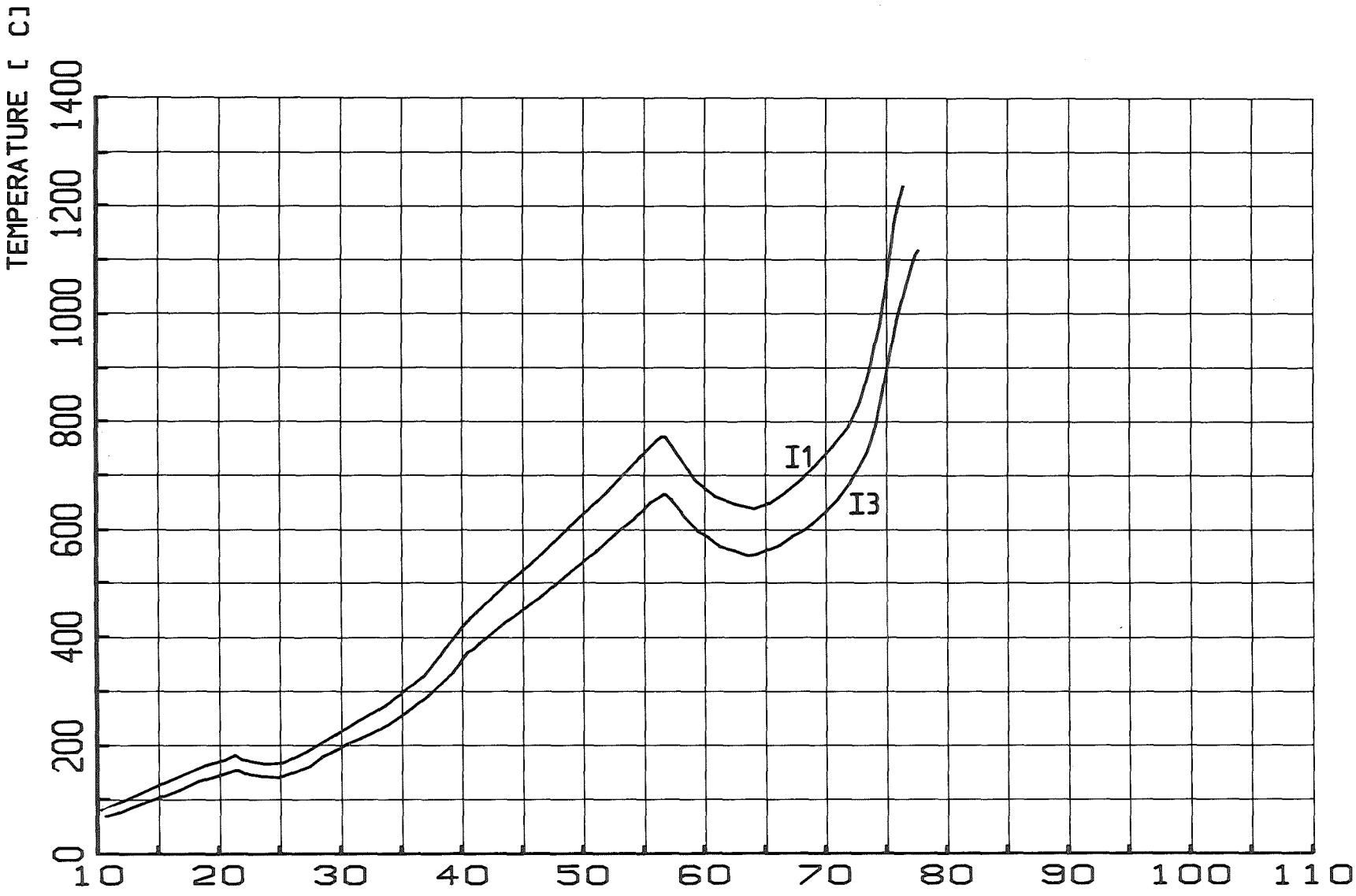

FIG. 43: TEMPERATURES IN THE INSULATION AT THE 155 MM (I) ELEVATION 1.3 MM (I1) AND 3.8 MM (I3) INTO THE FIBER CERAMIC. : ESBU-2A

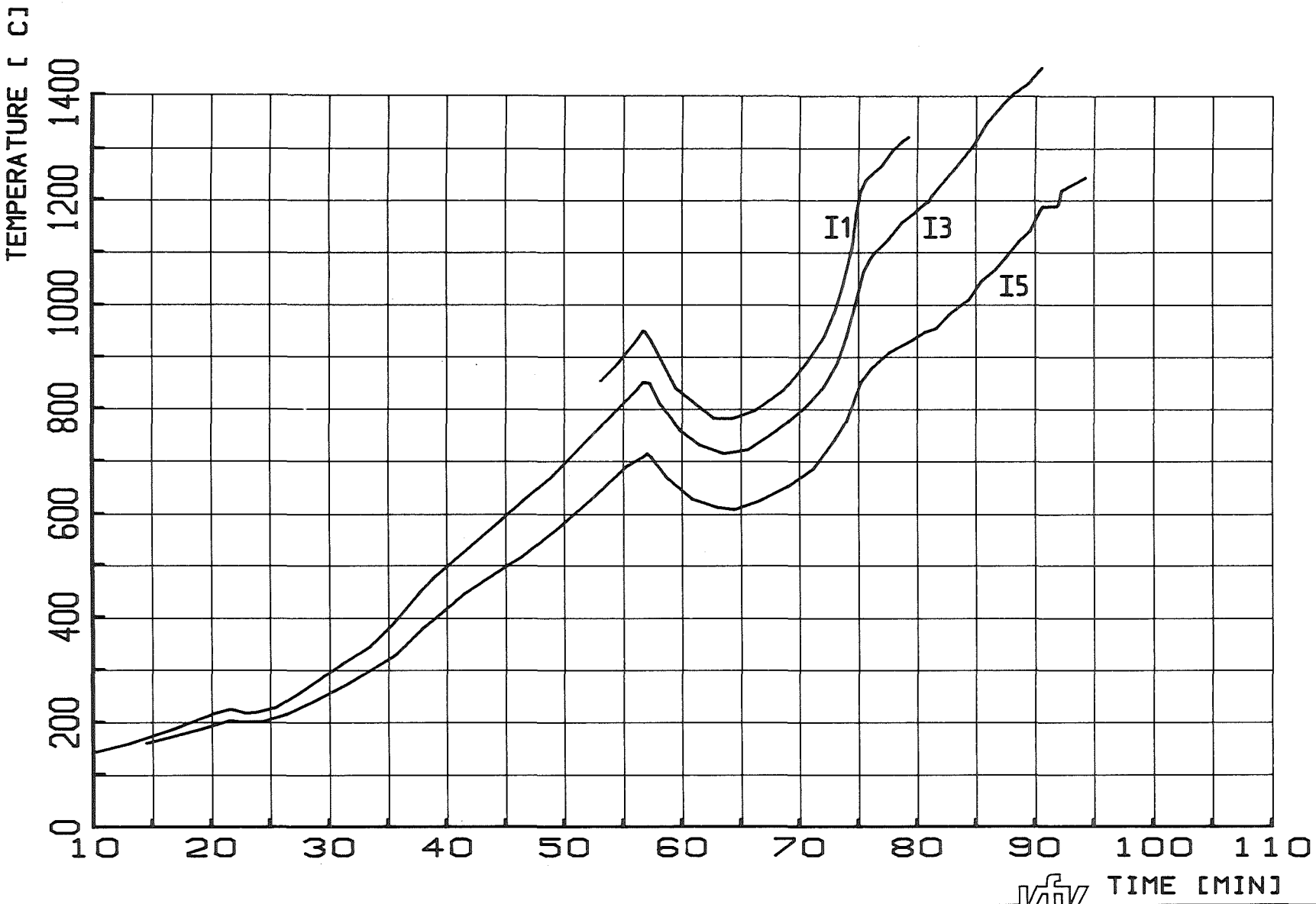

FIG. 44: TEMPERATURES IN THE INSULATION AT THE 255 MM (II) ELEVATION 1.3 MM (I1) AND 3.8 MM (I3) AND 6.4 MM (I5) INTO THE FIBER CERAMIC. : ESBU-2A

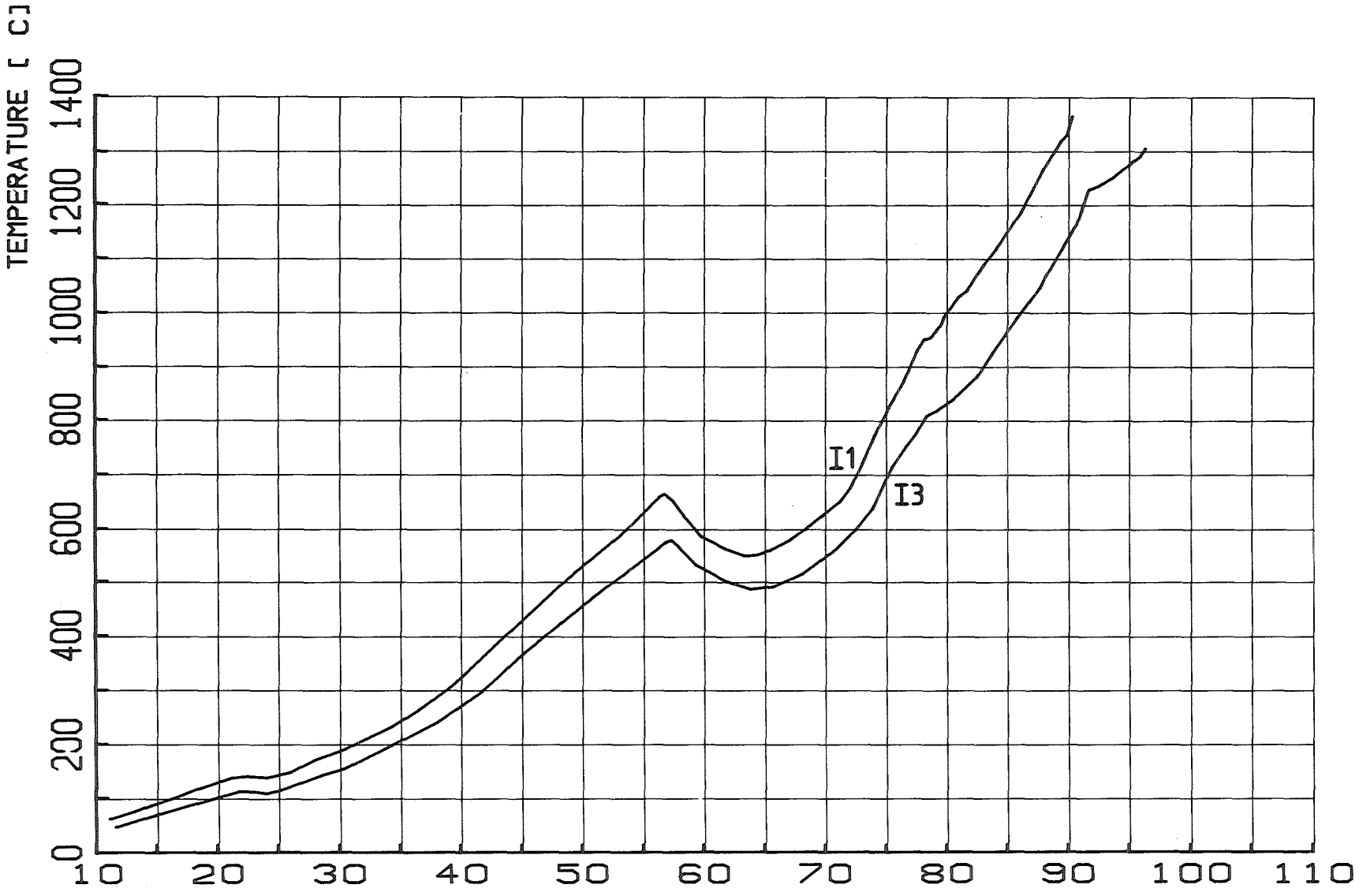

FIG. 45: TEMPERATURES IN THE INSULATION AT THE 345 MM (III) ELEVATION 1.3 MM (I1) AND 3.8 MM (I3) INTO THE FIBER CERAMIC. : ESBU-2A

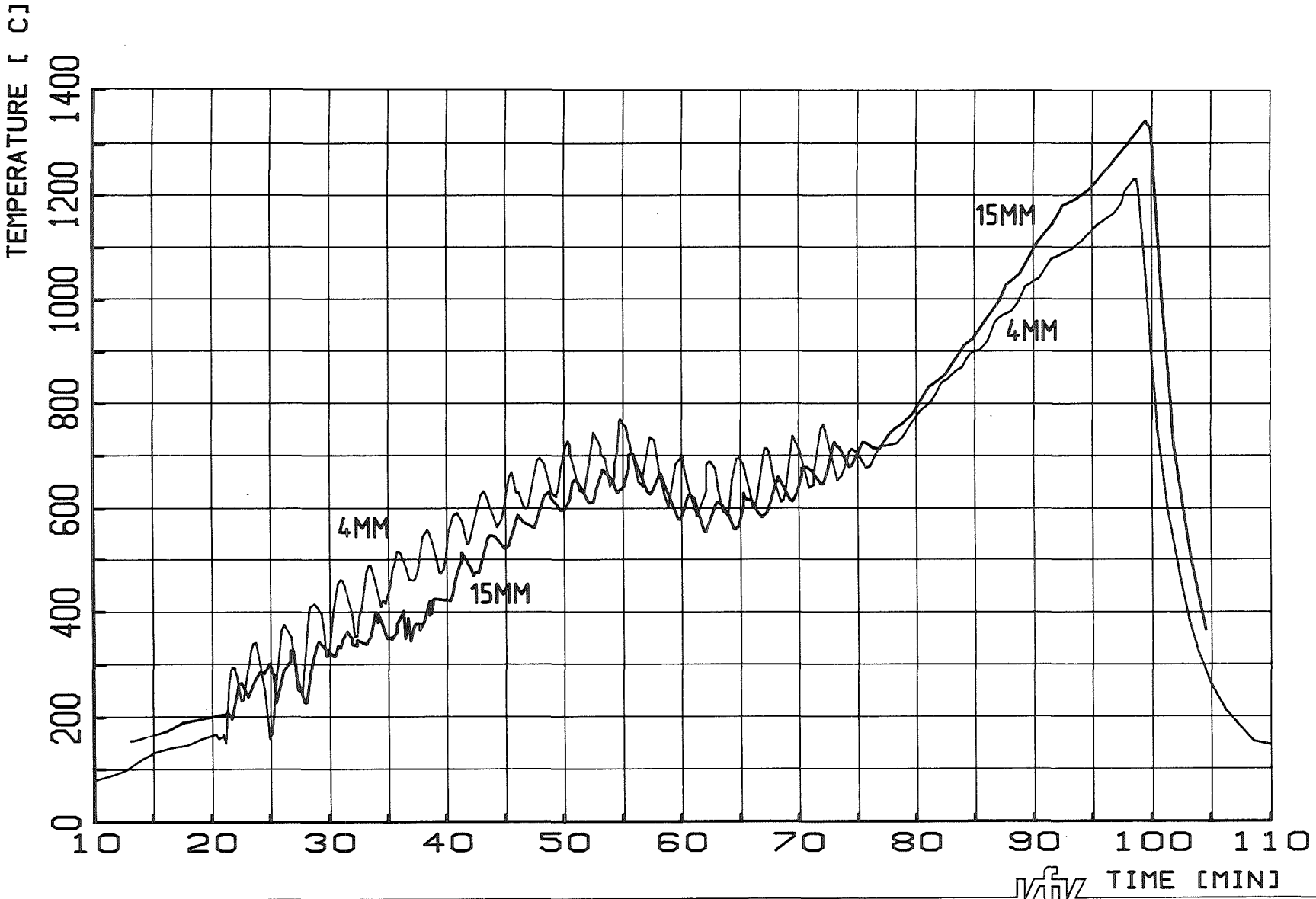

FIG. 46: STEAM TEMPERATURES AT 380 MM ABOVE THE LOWER END OF THE CLADDING AT A 4 MM AND A 15 MM RADIAL DISTANCE FROM THE SHROUD. : ESBU-2A

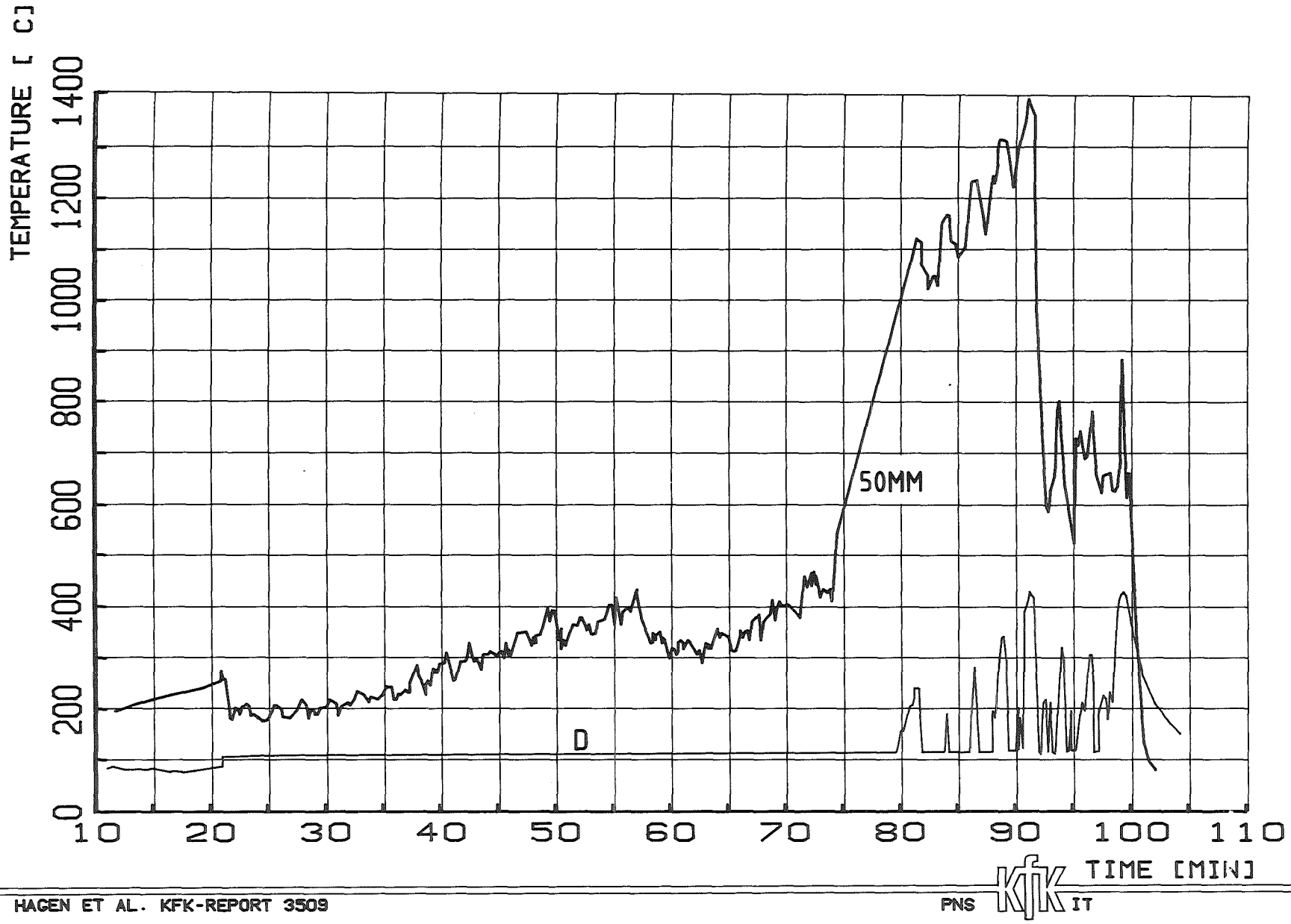

FIG. 47: STEAM TEMPERATURES AT 50 MM ABOVE THE LOWER END OF THE CLADDING AT A 15 MM RADIAL DISTANCE FROM THE SHROUD AND TEMPERATURE AT THE STEAM DISTRIBUTION SYSTEM (D). : ESBU-2A

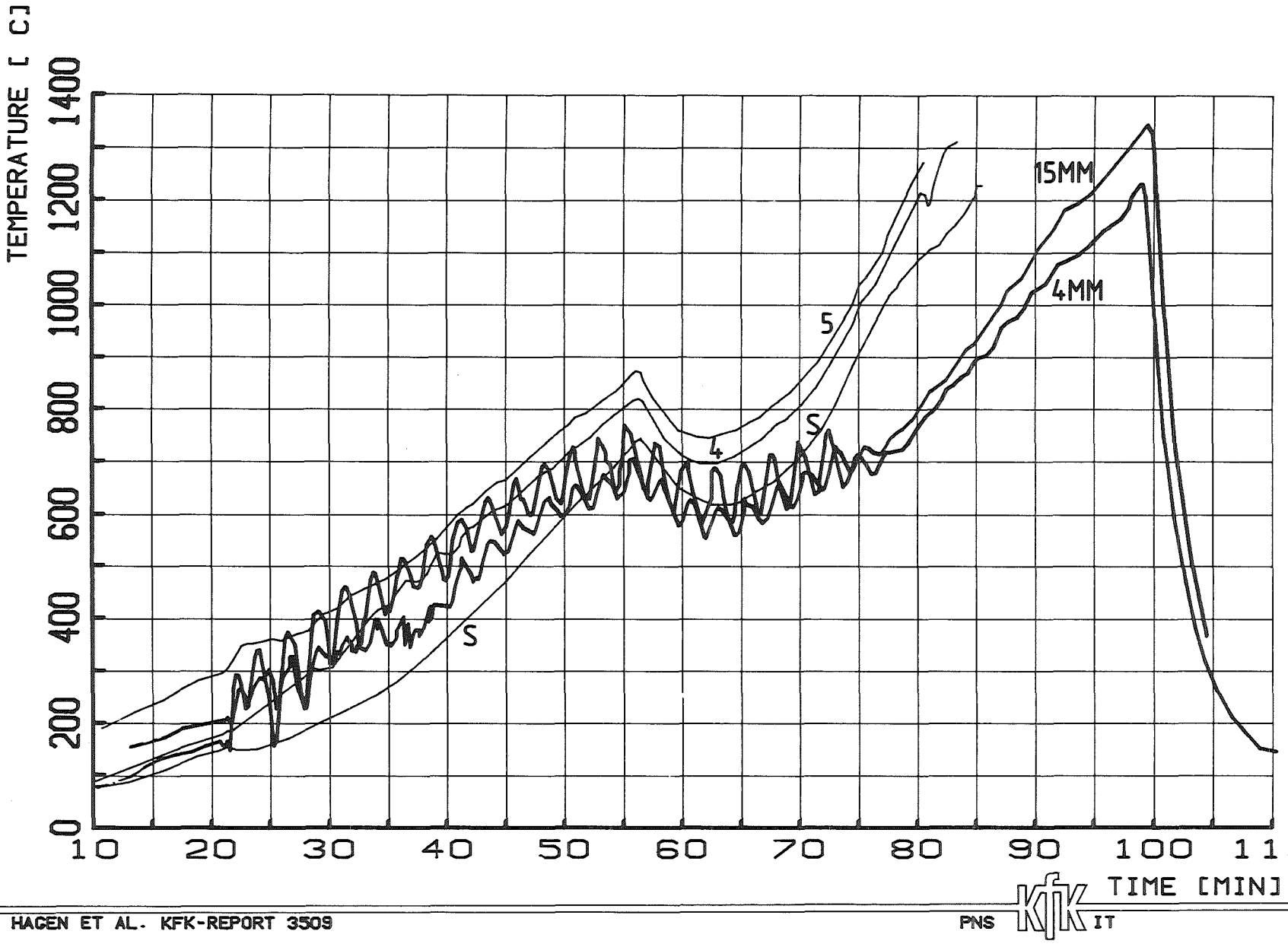

FIG. 48: STEAM TEMPERATURE AT 380 MM ABOVE THE LOWER END OF THE CLADDING AT A 4 MM AND A 15 MM RADIAL DISTANCE FROM THE SHROUD COMPARED TO THE TEMPERATURE ON THE CENTRAL ROD (5). SIDE ROD (4) AND SHROUD (S) AT 345 MM. : ESBU-2A

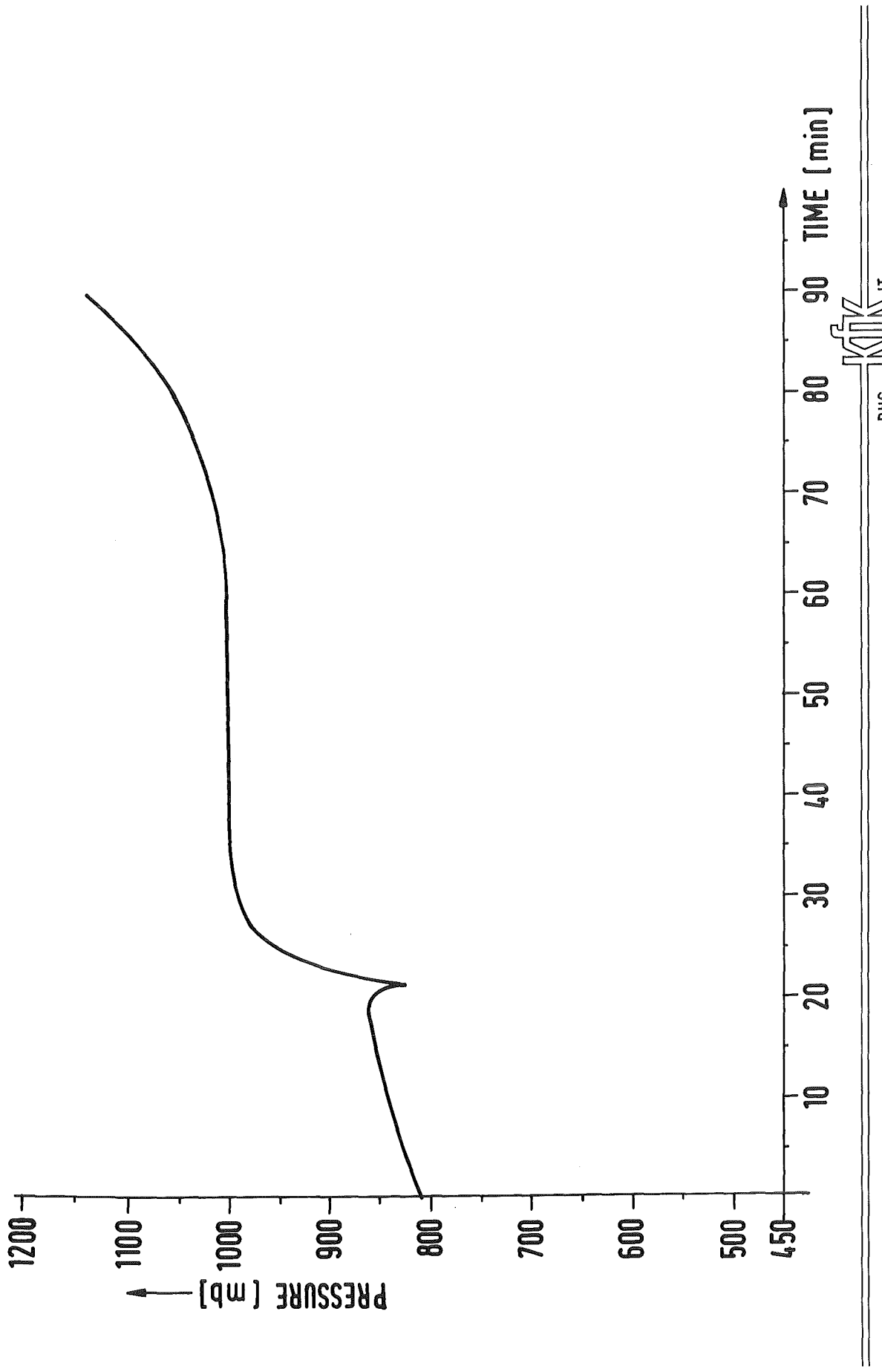

FIGIURE 49: PRESSURE IN THE TEST VESSEL FOR TEST ESBU-2A